Université du Québec

Institut National de la Recherche Scientifique

Centre Énergie, Matériaux et Télécommunication (INRS-EMT)

Generation of Ultrashort Laser Pulses via Vibrational Stimulated Raman Scattering and their Characterization using Frequency Resolved Optical Gating (FROG)

By

Shadieh Talaeinalous

A thesis submitted for the achievement of the degree of

Master of Science, M.Sc.

in Energy and Materials Sciences

Jury Members

Internal Examiner	Andreas Ruediger, INRS *INRS-EMT*
External Examiner	André Staudte *University of Ottawa*
Director of Research	François Légaré *INRS-EMT*

DEDICATION

This thesis is dedicated to my beloved parents; without their endless love and encouragement, I would never have been able to complete my graduate study.

This thesis is also dedicated to my cherished sisters, whose unwavering support and care have been invaluable throughout this path.

ACKNOWLEDGEMENTS

I am extremely fortunate to have completed my master's degree at the Institut National de la Recherche Scientifique (INRS), which is part of the Université du Québec. I am deeply grateful to my supervisor, Prof. François Légaré, for selecting me for this program and for his generous support, which includes granting me a full scholarship to offset the costs of my studies. Being asked to join his research team was a privilege. His patient assistance and perceptive observations provided me with the opportunity to deepen my knowledge more easily and encouraged me to do more and learn more constantly.

INRS conducted the work on this study. Many thanks to everybody who contributed their time and expertise throughout my career. Particularly, I would like to appreciate our post-doctoral researcher, Dr. Stephen Londo, and PhD student, Mayank Kumar, for all their assistance and for the exceptional work they have accomplished jointly on many projects. Their expertise, assistance, and technical understanding had a long-lasting impact on the accomplishments I attained in this path. I am deeply grateful to the professional team at the Advanced Laser Light Source (ALLS), Dr. Heide Ibrahim, and other technical team members for their willingness to share information and experience, which contributed to my progress. Their help and support taught me much. I also thank Dr. Reza Safaei and his group members, and my friend Pedram Abdolghader, for all their assistance.

Last but not least, I am thankful to my parents and sisters for always loving me, supporting me, and believing in me. Everything I have accomplished would not be possible without their unconditional support and encouragement.

ABSTRACT

High-power, ultrashort laser sources play a crucial role in a wide range of applications, including nonlinear frequency conversion, medical applications, ultrafast spectroscopy, and precision materials processing. Accessing ultrashort and tunable laser sources covering a different range of the spectrum using several ultrashort laser sources is not ideal due to cost and space limitations. As an alternative way, many systems employ nonlinear frequency conversion techniques—such as optical parametric amplification (OPA)—to extend tunability from a single laser source. However, OPA is a multistage setup, requiring precise alignment, phase-matching conditions, and synchronization between the pump and seed pulses to ensure stable and efficient operation. An alternative approach is using vibrational Stimulated Raman Scattering (SRS), which enables frequency shifting through molecular vibrations. In this thesis, we investigate the use of gas-filled hollow-core fibers (HCFs) as a platform for efficient SRS-based frequency conversion and pulse compression. This method enables the generation of high-energy, ultrashort pulses using methane (CH_4) as the Raman-active medium. The study focuses on the generation and characterization of ultrashort infrared laser pulses via vibrational SRS in gas-filled HCFs, with temporal and spectral diagnostics performed using Frequency-Resolved Optical Gating (FROG). Picosecond pump pulses were used to excite vibrational SRS while avoiding self-phase modulation (SPM) by broadening 60-fs initial pump pulses to up to 3 ps. First Stokes (FS) compression was optimized using a positively chirped dispersive element, such as ZnSe optical windows. This thesis highlights the effectiveness of CH_4 as a Raman-active medium for generating high-energy frequency-shifted near infrared (NIR) light sources. The approach enables the generation of high-energy, tunable femtosecond pulses, offering significant advantages for the development of compact and scalable ultrafast laser systems.

Keywords: Ultrafast lasers; Self-phase modulation (SPM); Stimulated Raman Scattering (SRS); First Stokes (FS); Frequency resolved optical gating (FROG); Hollow core fiber (HCF); Spectral broadening induced by Raman-active gases like Methane (CH_4).

RÉSUMÉ

Les sources laser ultracourtes de haute puissance jouent un rôle crucial dans un large éventail d'applications, notamment la conversion de fréquence non linéaire, les applications médicales, la spectroscopie ultrarapide et l'usinage de matériaux de précision. L'accès à des sources laser ultracourtes et accordables couvrant une gamme spectrale différente à l'aide de plusieurs sources laser ultracourtes n'est pas idéal en raison des contraintes de coût et d'espace. De nombreux systèmes utilisent des techniques de conversion de fréquence non linéaire, comme l'amplification paramétrique optique (APO), pour étendre l'accordabilité d'une source laser unique. Cependant, l'APO est une configuration à plusieurs étages, nécessitant un alignement précis, des conditions d'accord de phase et une synchronisation entre les impulsions de pompage et d'amorçage pour assurer un fonctionnement stable et efficace. Une autre approche consiste à utiliser la diffusion Raman stimulée par vibration (RSS), qui permet un décalage de fréquence par vibrations moléculaires. Dans cette thèse, nous étudions l'utilisation de fibres à cœur creux remplies de gaz (HCF) comme plateforme pour une conversion de fréquence et une compression d'impulsions efficaces basées sur la SRS. Cette méthode permet de générer des impulsions ultracourtes de haute énergie en utilisant le méthane (CH_4) comme milieu actif Raman. L'étude se concentre sur la génération et la caractérisation d'impulsions laser infrarouges ultracourtes par SRS vibrationnelle dans des HCF remplis de gaz, avec des diagnostics temporels et spectraux effectués par FROG (Frequency-Resolved Optical Gating). Des impulsions de pompe picosecondes ont été utilisées pour exciter la SRS vibrationnelle tout en évitant l'automodulation de phase (SPM) en élargissant les impulsions de pompe initiales de 60 fs jusqu'à 3 ps. La compression First Stokes (FS) a été optimisée à l'aide d'un élément dispersif à dérive de fréquence positive, comme des fenêtres optiques en ZnSe. Cette thèse met en évidence l'efficacité du CH_4 comme milieu actif Raman pour générer des sources lumineuses infrarouge proche décalées en fréquence de haute énergie. Cette approche permet la génération d'impulsions femtosecondes accordables de haute énergie, offrant des avantages significatifs pour le développement de systèmes laser ultrarapides compacts et évolutifs.

Mots-clés : Lasers ultrarapides ; Automodulation de phase (SPM) ; Diffusion Raman stimulée (SRS) ; Premier Stokes (FS) ; Déclenchement optique résolu en fréquence (FROG) ; Fibre à cœur creux (HCF) ; Élargissement spectral induit par des gaz actifs en Raman comme le méthane (CH_4).

SYNOPSIS

Génération d'impulsions laser ultracourtes par diffusion Raman stimulée par vibration et leur caractérisation à l'aide de la modulation optique à fréquence résolue

Actuellement parmi les instruments les plus sophistiqués en photonique, les lasers ultrarapides peuvent générer des impulsions électromagnétiques d'une durée allant de quelques femtosecondes (1 fs = 10^{-15}secondes) à plusieurs picosecondes (1 ps = 10^{-12}) [1, 2]. Dans les opérations de micro-fabrication de haute précision, ces impulsions très courtes sont absolument cruciales car elles permettent des approches impossibles avec les techniques d'usinage conventionnelles. Alors que les impulsions ultrarapides les plus longues s'étendent dans la gamme des picosecondes, les impulsions attosecondes (1 as = 10^{-18}) [3, 4] sont la frontière de la science ultrarapide, désignant la lumière détectable la plus courte. En raison de leur capacité à étudier et à contrôler les matériaux à des échelles de temps ultrarapides, les impulsions laser ultracourtes ont révolutionné le domaine de l'optique et de la photonique. L'objectif de cette thèse est de générer de telles impulsions par diffusion Raman stimulée par vibration (SRS) dans des fibres à cœur creux remplies de gaz (HCF) et de les caractériser temporellement et spectralement par modulation optique en fréquence. L'objectif est de développer des méthodes de compression d'impulsions efficaces permettant la réalisation de lasers femtosecondes compacts et à haute énergie. La thèse explore les concepts physiques, les techniques expérimentales et l'optimisation de la correction de dispersion pour générer des impulsions bien compressées, d'une durée d'environ 180 fs.

Contexte théorique des impulsions ultracourtes et de l'amplification par dérive de fréquence

Les méthodes de verrouillage de mode des années 1960 ont marqué le début de la génération d'impulsions ultracourtes [5]. Au fil des ans, des développements tels que le verrouillage de mode par lentille Kerr et l'amplification par dérive de fréquence (CPA) en 1985 [6, 7] ont permis aux scientifiques de réduire la durée des impulsions à quelques femtosecondes. L'amplification par dérive de fréquence est fondamentale pour produire des impulsions laser ultracourtes de haute intensité. La CPA a propulsé la technologie laser Ti:Saphir au point que la production d'impulsions multimillijoules inférieures à 50 fs est désormais une pratique courante [8]. L'autofocalisation limite l'amplification des impulsions laser ultracourtes. L'impulsion est d'abord étirée à l'aide d'une ligne à retard à dispersion positive avant amplification. Ensuite, une ligne à retard à dispersion négative comprime l'impulsion pour la ramener à sa forme initiale [6]. Une impulsion courte et de faible énergie est étirée intentionnellement à l'aide d'un

extenseur – dans ce cas, la propagation dans une fibre optique monomode – pour générer une impulsion étirée. L'impulsion est modulée linéairement dans la fibre par automodulation de phase (section 3.2) combinée à une dispersion de vitesse de groupe. Ensuite, un compresseur à double réseau amplifie l'impulsion étirée puis la compresse. Des niveaux d'énergie plus élevés avant l'autofocalisation sont obtenus en augmentant l'impulsion étirée plutôt que l'impulsion compressée. Les lasers solides ultrarapides de haute puissance, en particulier ceux utilisant de minuscules tiges de saphir dopé au titane comme milieu de gain, offrent des avantages substantiels grâce à leurs énergies d'impulsion élevées, leur puissance de sortie supérieure et leurs durées d'impulsion plus courtes que les lasers à colorant. Il est donc difficile d'augmenter leur puissance moyenne, car un pompage direct efficace par diode est impossible. Leur conception complexe, notamment pour générer des impulsions de forte énergie et de courte durée, réduit également leur utilité en milieu industriel.

Grâce à leur large bande passante de gain, les lasers Ti: Saphir sont devenus la référence absolue pour la génération de telles impulsions. Leur large bande passante, généralement comprise entre 650 et 1100 nm, les rend parfaits pour les applications nécessitant une mise en forme précise des impulsions et une résolution temporelle exceptionnelle [4]. La génération d'impulsions ultracourtes dépend de cette large bande passante, qui permet également de produire des impulsions aussi courtes que 10 femtosecondes. En comparaison, les lasers à fibre (lasers dopés à l'ytterbium) ont des bandes passantes de gain plus focalisées, autour de 1030 nm. Les systèmes à base d'ytterbium offrent divers avantages malgré leur bande passante plus faible, notamment une meilleure gestion thermique, une plus grande efficacité et une puissance de sortie moyenne potentiellement plus élevée. Ces caractéristiques les rendent particulièrement adaptés aux applications industrielles, où l'efficacité et la durabilité sont des préoccupations majeures.

Les bases théoriques des lasers à impulsions ultracourtes incluent des phénomènes optiques non linéaires comme l'auto modulation de phase (SPM) [9] et la compensation de dispersion à l'aide de miroirs à dérive de fréquence. Ces idées permettent le contrôle et la structuration temporelle des impulsions, où une excellente résolution temporelle est essentielle pour étudier la dynamique moléculaire. Les lasers ultrarapides sont utilisés en spectroscopie, en imagerie biomédicale, en micro-fabrication et en science de l'attoseconde.

Nombreux sont ceux qui attribuent à Paul Corkum et Ferenc Krausz, au début des années 2000 [16, 22], les efforts pionniers de la première génération d'impulsions attosecondes. Ces impulsions ultracourtes ont été générées grâce à leurs travaux sur la génération d'harmoniques d'ordre élevé (HHG) en milieu gazeux,

ce qui leur a permis d'étudier les processus physiques ultrarapides et de découvrir des phénomènes optiques non linéaires sophistiqués, notamment la filamentation optique.

Les impulsions ultrarapides, avec leurs durées étonnamment courtes, peuvent atteindre des intensités maximales de l'ordre de 10^{12} W/cm², même à de faibles puissances moyennes. Elles sont idéales pour l'étude de la dynamique ultrarapide atomique et moléculaire. Les progrès technologiques dans la production d'impulsions, notamment l'utilisation de lasers à colorant à large spectre d'émission, ont permis de réduire la durée des impulsions à quelques centaines de femtosecondes seulement. Les développements ultérieurs ont repoussé ces limites encore plus loin, permettant des impulsions inférieures à 10 femtosecondes dans les années 1980, les préparant ainsi à des utilisations scientifiques et industrielles étendues.

Concept laser et optique non linéaire

Les lasers fonctionnent sur l'inversion de population et l'émission stimulée. La génération d'impulsions ultracourtes dépend des larges spectres d'émission fournis par les lasers à solide tels que les lasers à fibre dopée Ti: Saphir et Yb. En optique non linéaire (NLO), le comportement de la lumière dans les milieux non linéaires où la densité de polarisation P montre une réponse non linéaire au champ électrique E de la lumière est étudié. Ce comportement non linéaire devient évident à de très fortes intensités lumineuses, généralement lorsque le champ électrique de la lumière dépasse 10^8 V/m, atteignant ainsi des valeurs équivalentes au champ électrique atomique d'environ 10^{11}V/m souvent généré par les lasers dans de telles circonstances. [10]. La lumière laser de haute intensité interagissant avec un matériau non linéaire produit une SPM, une diffusion Raman et d'autres processus de conversion de fréquence qui permettent une extension des capacités laser au-delà des limites traditionnelles et la production d'harmoniques, entre autres effets. Alors que la dispersion doit être contrôlée pour comprimer. La SPM est utilisée pour l'élargissement spectral. Les fibres à cœur creux laissent la lumière traverser les milieux gazeux et la limitent spatialement, améliorant ainsi les effets non linéaires sur des durées d'interaction plus longues. Associés à des gaz actifs en Raman comme le méthane, ces guides d'ondes sont essentiels à l'amplification et à la compression des impulsions SRS.

Effet Kerr, auto modulation de phase et dispersion de vitesse de groupe

L'effet SPM, découvert au début de la recherche en optique non linéaire [9, 11], est un phénomène qui se produit lorsqu'un faisceau optique intense traverse un milieu Kerr. Le milieu Kerr est un matériau dont l'indice de réfraction change en réponse à l'intensité de la lumière qui le traverse, ce qui provoque une

modulation de phase proportionnelle à sa distribution d'intensité en raison de sa non-linéarité. Le HCF rempli de gaz, signalé pour la première fois dans les fibres optiques en 1978 [38], en tant que milieu non linéaire, offre une plateforme appropriée pour les recherches expérimentales car il permet des effets non linéaires significatifs sans variations spatiales ou thermiques (détails dans la section 3.4) [31]. La propagation de la lumière à l'intérieur d'une fibre entraîne une variation infime de l'indice de réfraction (IR) de la fibre. Lorsque le champ électromagnétique de la lumière interagit avec les atomes et les molécules du milieu, un phénomène connu sous le nom d'effet Kerr se produit. Une paire de transformées de Fourier décrit les domaines temporel et fréquentiel inversement connectés d'une impulsion laser. Cette relation implique que des durées d'impulsion plus courtes correspondent à des bandes passantes spectrales plus larges. Maximiser la largeur de bande de fréquence permettra de produire des impulsions courtes correspondantes dans le temps grâce au SPM. Le SPM génère de nouvelles fréquences dans une large gamme [39]. Comme l'indice de réfraction du verre (IR) change sous l'effet Kerr, la partie médiane, le bord de fuite et le bord d'attaque diffèrent légèrement. Cette variation influence la phase des ondes lumineuses formant l'impulsion, affectant ainsi la fréquence. Comme le montre la figure 3-1, le spectre de fréquence de l'impulsion s'élargit ainsi, les fréquences les plus basses apparaissant sur le bord d'attaque et les fréquences les plus élevées sur le bord de fuite. Le spectre de l'impulsion s'élargit toujours sur la fibre [39]. Au centre de l'impulsion, le chirp positif créé par le SPM est observé de manière presque linéaire, produisant un chirp (un lent décalage de fréquence) sur toute la période de l'impulsion. Généralement, la forme de l'impulsion et le premier chirp ajouté à l'impulsion définissent le spectre. Si le même chirp est présent à deux moments distincts, l'impulsion a la même fréquence instantanée aux deux endroits. Ces points montrent essentiellement deux ondes de même fréquence mais de phases différentes, qui, selon leur déphasage relatif, peuvent interagir de manière constructive ou destructive. En raison de cette interférence, le spectre d'impulsions présente une structure oscillante caractéristique [39, 40]. La SPM a initié des recherches approfondies sur les phénomènes optiques non linéaires. Dans le cas d'un faisceau pulsé d'entrée, le changement de phase temporel de la SPM modifie le spectre optique. La modulation de fréquence (chirp) du champ électrique de l'impulsion façonne ce changement : la SPM induit un élargissement du spectre si l'impulsion est initialement limitée par transformée de Fourier (FTL) ou chirpée vers le haut. En revanche, la SPM provoque une compression spectrale dans une impulsion initialement chirpée vers le bas [38, 41]. Dans des conditions de SPM intense, le spectre optique peut présenter des oscillations notables. Lorsqu'un champ électrique « E » est introduit dans un milieu diélectrique transparent, il déforme la distribution des charges électroniques au sein du milieu. Cette distorsion mène à une polarisation induite « P » dans le milieu, qui, en première approximation, présente

une linéarité en réponse au champ « E » appliqué. Cependant, sous l'influence d'un champ électrique « E » intense, la réponse de polarisation au champ appliqué peut s'écarter de la linéarité. [35].

En optique ultrarapide, la dispersion est essentielle, car son type détermine si les impulsions sont étirées ou comprimées. La mise en forme optimale des impulsions dépend de la gestion de la dispersion de vitesse de groupe (GVD) et des termes de dispersion d'ordre supérieur. Les miroirs à dérive de fréquence, les paires de réseaux et les géométries de fibres personnalisées permettent de compenser la largeur et la phase des impulsions [12].

Le produit temps-bande passante (TBP) établit des limites théoriques pour la compression des impulsions et définit une relation entre la résolution temporelle et la résolution spectrale. Certains systèmes générant des impulsions inférieures à 10 fs, des techniques telles que le verrouillage de mode par lentille Kerr et l'élargissement du spectre dans les fibres à gaz ont permis d'allonger la durée des impulsions jusqu'à quelques femtosecondes. L'étude des événements ultrarapides en physique, en chimie et en biologie requiert de telles capacités, ce qui fait de l'optique non linéaire un élément fondamental du développement de systèmes laser ultrarapides.

Fibre à noyau creux

Cette thèse comprend une revue approfondie des avancées récentes en optique non linéaire, avec un accent particulier sur l'utilisation de HCF remplies de gaz pour la génération et la compression d'impulsions laser ultracourtes. Ces guides d'ondes, caractérisés par leur cœur creux et leur gaine diélectrique, permettent d'améliorer les longueurs d'interaction non linéaire et de produire des impulsions aussi courtes que 4,5 femtosecondes [13]. Les caractéristiques fondamentales des HCF et leurs avantages par rapport aux fibres à cœur plein conventionnelles, notamment en termes d'accord de phase et de faible dispersion du matériau, sont abordés.

L'indice de réfraction dépendant de l'intensité du milieu (l'effet Kerr) provoque un SPM qui génère des déphasages tout au long de l'impulsion. Un spectre d'impulsion intense s'élargit lors de sa traversée d'un milieu Kerr tel qu'une HCF remplie de gaz en raison de la variation de l'indice de réfraction. Des méthodes de compensation de dispersion peuvent ensuite être utilisées pour compresser ce spectre élargi et générer des impulsions ultracourtes. La dynamique de propagation de la lumière est étudiée à l'aide de l'approximation paraxiale et de la structure modale des fibres multimodes, en particulier des modes LP [13].

Dans cette thèse, le couplage des modes et l'influence de la polarisation dans les fibres multimodes ont été étudiés. Les modes LP_{01} et LP_{11} prédominent dans de nombreuses applications pratiques. Chaque mode possède une constante de propagation et un profil d'intensité spatiale distincts. Par exemple, la symétrie du mode LP_{01} le rend idéal pour une dispersion minimale et un transfert d'énergie efficace. La conception de systèmes de fibres capables de fournir des impulsions stables et à haute énergie repose sur la connaissance de la façon dont les différents modes interagissent et évoluent à l'intérieur de la fibre [13].

Porte optique résolue en fréquence

La méthode FROG (Frequency Résolve Optical Gating), introduite par Rick Trebino en 1993, exploite toute réponse optique non linéaire quasi immédiate [14]. Elle permet de caractériser pleinement les impulsions laser ultracourtes, en mesurant l'intensité et la phase en fonction du temps ou de la fréquence, grâce à des interactions optiques non linéaires. Contrairement aux techniques d'autocorrélation conventionnelles, la méthode FROG permet de reconstituer intégralement l'intensité et la phase d'une impulsion. Elle consiste à diviser l'impulsion en deux copies identiques et à les diriger à travers un élément optique non linéaire avec un délai contrôlable entre les copies. Le signal non linéaire est ensuite analysé spectralement en fonction de cette différence de temps. L'analyse spectrale du signal résultant en fonction du délai produit un spectrogramme bidimensionnel appelé trace FROG. Les équations du champ de signal et l'enregistrement des traces SHG-FROG sont entièrement clarifiés. [14, 15].

Types de FROG

Des comparaisons sont effectuées entre plusieurs types de FROG : SHG, THG, PG, SD et TG. Malgré son incertitude temporelle et directionnelle, le SHG-FROG est privilégié pour sa sensibilité et sa simplicité. Cependant, ces techniques nécessitent des configurations plus sophistiquées et des techniques de troisième ordre, car les FROG PG et SD fournissent des traces plus claires et éliminent l'incertitude. Bien que très sensible, le FROG à réseau transitoire nécessite plusieurs faisceaux et un alignement précis, ce qui limite son application pratique [16].

L'approche par projection généralisée visant à surmonter les contraintes des algorithmes FROG fondamentaux a été présentée. Opérant dans l'espace des fonctions définies sur les champs de signaux, cette méthode itérative impose deux contraintes : la trace FROG expérimentale et la réalisabilité physique de l'impulsion. Cette approche optimise l'approximation du champ électrique complexe en alternant projections fréquentielles et temporelles. Même pour des formes d'impulsions très complexes, cette approche garantit la convergence et augmente la précision de la récupération d'impulsions. Enfin, des

traces FROG enregistrées et reconstruites d'impulsions laser Ti: Saphir sont présentées à partir des résultats expérimentaux du laboratoire ALLS. Ces résultats confirment l'efficacité de la compression basée sur HCF et de la caractérisation SHG-FROG pour la génération et l'analyse d'impulsions laser à quelques cycles. Le chapitre conclut en soulignant les possibilités futures de fusion de méthodes sophistiquées de mise en forme d'impulsions avec des diagnostics en temps réel tels que FROG, en vue de la science de l'attoseconde et au-delà.

Notions de base sur la diffusion Raman stimulée (SRS)

Il existe deux types de diffusion élastique selon la taille des particules diffusantes : la diffusion de Mie et la diffusion de Rayleigh [17]. La diffusion de Mie se produit lorsque la lumière de toutes les fréquences est diffusée uniformément avec une taille de particule supérieure à la lumière incidente, quelle que soit la longueur d'onde. En revanche, la diffusion de Rayleigh se produit lorsque la taille de la matière est bien inférieure à la longueur d'onde de la lumière incidente. Selon la longueur d'onde de la lumière incidente, la différence réside dans le degré de diffusion. La couleur bleue du ciel résulte de la diffusion de Rayleigh. La plupart du temps, les photons frappent une molécule de manière élastique (diffusion de Rayleigh) avec une longueur d'onde inchangée par rapport à la lumière incidente. Cependant, il existe une diffusion inélastique dans laquelle quelques photons se diffusent de telle sorte que la longueur d'onde de la lumière diffusée est modifiée en raison de l'interaction avec une molécule. En 1928, le physicien C. V. Raman a découvert la diffusion Raman, une diffusion inélastique [17]. Lors d'une telle diffusion Raman, la longueur d'onde de la lumière peut diminuer ou augmenter, ce qu'on appelle respectivement diffusion Raman Stokes ou anti-Stokes [17].

Le terme SRS désigne un ensemble de techniques optiques dans lesquelles deux champs lumineux induisent une transition Raman-active dans une substance [26]. La SRS est couramment utilisée depuis les années 1960 pour étudier les propriétés vibrationnelles des gaz, des liquides et des solides, y compris celles des liaisons et des groupes chimiques, qui utilisent les mêmes vibrations moléculaires que la diffusion Raman spontanée. Cela permet d'étudier la dynamique structurale et les interactions des molécules, ainsi que de les identifier. La SRS génère un rayonnement directionnel et intense en générant de manière cohérente des modes vibrationnels, semblables mais différents des mouvements moléculaires incohérents provoqués par la diffusion Raman spontanée. La SRS offre une efficacité de détection du signal bien supérieure à celle de la diffusion Raman naturelle. De plus, elle permet l'observation directe des mouvements cohérents des molécules à des échelles de temps ultrarapides, fournissant des informations sur les processus et la dynamique moléculaire, difficilement observables par la seule analyse des spectres

Raman. De plus, la grande sensibilité des signaux Raman et la capacité à résoudre les mouvements moléculaires dans le temps ont fait de la SRS un instrument précieux en imagerie biomoléculaire, en biologie et en chimie [26].

La diffusion de la lumière stimulée résulte d'une modification des caractéristiques optiques du matériau induite par le champ optique. Cela induit une relation non linéaire entre les différentes composantes du champ par une certaine forme d'excitation au sein du matériau, entraînant des modifications de ses propriétés optiques. Cette non-linéarité est généralement caractérisée par une susceptibilité complexe et une polarisation non linéaire du troisième ordre concernant les champs en interaction.Une description détaillée de la diffusion Raman stimulée (SRS) [17] a été présentée. Grâce à l'interaction cohérente de la lumière avec les vibrations moléculaires, ce processus optique non linéaire produit de nouvelles composantes fréquentielles. L'énergie du photon diffusé, plus ou moins élevée que celle du photon d'origine, détermine la production de composantes Stokes et anti-Stokes. Cette thèse explique comment exploiter la SRS grâce à des fibres à cœur creux pour générer des impulsions comprimées avec décalage de fréquence. En considérant les composantes réelles et imaginaires de la susceptibilité du troisième ordre, les équations couplées non linéaires fournissent la théorie classique de la SRS. Il en résulte des équations de gain prédisant l'amplification exponentielle du signal Stokes en conditions d'accord de phase. La SRS résulte de l'interaction d'un laser de pompage avec les modes vibrationnels d'un milieu, générant ainsi des composantes décalées vers le rouge (Stokes) et vers le bleu (anti-Stokes). La SRS vibrationnelle transfère de l'énergie pour produire des impulsions Stokes cohérentes lorsque la différence de fréquence entre deux faisceaux rencontre une fréquence de vibration moléculaire. L'activité Raman rend le méthane utile dans ce travail. La thèse étudie les première et deuxièmes composantes de Stokes. Le traitement théorique repose sur des équations couplées non linéaires décrivant les conditions d'accord de phase et le transfert d'énergie.

Diffusion dans les fibres à cœur creux

Cette thèse présente une revue complète des recherches expérimentales et théoriques sur la SRS dans les HCFs, en se concentrant sur le décalage de fréquence, la compression d'impulsions et les processus optiques non linéaires dans des environnements remplis de méthane. Grâce à l'interaction entre de fortes impulsions laser et les modes vibrationnels des molécules de gaz, la SRS est un phénomène optique non linéaire qui permet la génération de nouvelles fréquences. La géométrie contrainte des fibres à cœur creux et l'environnement gazeux régulé améliorent les phénomènes non linéaires tels que la SRS et l'auto-modulation de phase. À faible énergie d'entrée, Benabid et al. [18] ont montré la SRS dans des fibres à

cristaux photoniques remplies d'hydrogène, générant ainsi efficacement un effet Stokes. Leurs résultats jettent les bases de recherches analogues utilisant d'autres gaz, dont le méthane, que cette thèse étudie. En utilisant des HCF remplies d'hydrogène, Chen et al. Ont observé des changements d'auto-fréquence des solitons, soulignant ainsi l'interaction entre la dynamique des solitons et la SRS. Ces résultats soulignent la nécessité du choix du gaz et de la mise en forme des impulsions dans les tests de SRS.

Configuration expérimentale

Des expériences ont été menées au laboratoire ALLS (Advanced Laser Light Source) à l'aide d'un laser Ti: Saphir de 780 nm avec une durée d'impulsion initiale de 60 fs. Une méthode de réseau de diffraction a permis d'élargir l'impulsion jusqu'à 3 ps. La compression du premier Stokes a été optimisée en utilisant une combinaison d'un élément dispersif à chirp positif, tel que des fenêtres optiques en ZnSe. Grâce à FROG, la caractérisation de l'impulsion a permis d'obtenir des profils d'intensité et de phase complets. Afin d'optimiser la compression de l'impulsion et le transfert d'énergie, des variables expérimentales telles que la pression du gaz, la position du réseau et le choix des composants optiques ont été systématiquement modifiées.

Les mesures de transmission de base et les caractérisations d'impulsions ont été effectuées sous vide. L'enregistrement de l'énergie d'entrée et de sortie a permis de calculer l'efficacité de transmission pour chaque configuration. Des filtres optiques (LP1000, SP1325, SP1319) ont été utilisés pour suivre la présence de composantes Stokes et anti-Stokes lors de l'injection de méthane à différentes pressions (1000 à 3000 mbar). La durée d'impulsion, les profils d'intensité et les propriétés de phase des impulsions transmises et produites ont été récupérés par FROG. L'impulsion Stokes initiale a confirmé une forte interaction non linéaire et une compensation efficace de la dispersion à une pression de méthane de 3000 mbar. Avec de faibles variations de la valeur efficace (RMS), le rendement de conversion énergétique de la première composante Stokes a atteint 10.6 %, suggérant une grande stabilité et une grande répétabilité. Bien qu'ils aient montré une plus grande instabilité et des longueurs d'impulsion plus longues, des signaux Stokes et anti-Stokes secondaires ont été observés à des pressions et une énergie plus élevée.

Le rendement de conversion a été déterminé au moyen des rapports de longueur d'onde et d'énergie ; la distribution d'énergie entre les impulsions Stokes de base, première et seconde a été examinée. Dans des conditions idéales, l'efficacité du second Stokes est restée d'environ 5.41 %. L'élargissement spectral observé sur les traces FROG a validé l'existence d'influences SPM et non linéaires. Des largeurs de bande spectrales plus importantes sont associées à des durées d'impulsion plus courtes. L'isolation des

composantes Stokes et l'ajustement des distributions d'énergie ont été fortement influencés par les paramètres de filtrage. Les premier et second signaux Stokes ont été séparés respectivement par une combinaison de LP1000 et SP1325 et une combinaison de LP1000 LP1319. La durée de l'impulsion et l'énergie totale étaient également affectées par la position du réseau. Les traces FROG récupérées et expérimentales correspondaient étroitement, vérifiant ainsi la fiabilité de l'algorithme de récupération de phase et la qualité de l'alignement. Parfois, un faible chirp et une asymétrie du profil temporel étaient observés, suggérant une dispersion résiduelle ou un alignement défectueux. Les ajustements de la lame d'onde n'avaient aucun impact sur la durée de l'impulsion et la polarisation. Les graphiques de phase spectrale montraient des changements de phase non linéaires conformes à l'effet Kerr et à l'interaction Raman. La deuxième impulsion Stokes a été récupérée grâce à une combinaison de filtres LP1000 et SP1319, avec une plage de 384 fs à 790 fs, ce qui a confirmé l'efficacité, mais la stabilité de la forme d'impulsion en fonction de l'énergie et de la pression. Enfin, la SRS dans les HCF remplis d'éthane est une technique performante pour produire des impulsions ultracourtes et contrôlables. Des durées d'impulsion inférieures à 200 fs ont été obtenues et caractérisées avec précision grâce à des ajustements appropriés de la pression, du filtrage et de la dispersion. La synchronisation optique à résolution de fréquence (FROG) permet la récupération complète de l'intensité et de la phase de l'impulsion dans le domaine temporel. Dans cette thèse, nous avons utilisé SHG-FROG pour enregistrer des traces temps-fréquence à l'aide d'un spectromètre et d'un cristal BBO. L'algorithme de récupération FROG reconstitue avec une grande précision les formes d'impulsion. Différentes configurations ont produit plusieurs traces expérimentales, avec une durée d’environ 180 fs pour la plus courte impulsion obtenue. Nous avons pu générer une impulsion ultracourte du premier Stokes avec un facteur de compression d’environ 17, et du second Stokes avec un facteur de compression de 4.

Effets des paramètres et optimisation

La position des réseaux, l'énergie d'entrée et la pression du gaz ont eu un impact significatif sur les caractéristiques des impulsions. L'augmentation de la pression a permis d'obtenir des performances SRS supérieures, tout en permettant un contrôle précis de la dispersion. Alors qu'une épaisseur plus importante (16 mm) créait d'importantes distorsions de phase, une épaisseur de fenêtre en ZnSe comprise entre 5 et 11 mm a permis d'obtenir des performances équilibrées. Avec un minimum d'erreurs, les traces FROG ont permis de vérifier la récupération des impulsions. Les interactions non linéaires ont également été confirmées par les signaux anti-Stokes observés. Les connaissances acquises ici contribuent à la création de petits systèmes femtosecondes à haute énergie pour la conversion de fréquence non linéaire,

la communication et la spectroscopie ultrarapide. Cette thèse offre un solide aperçu théorique et expérimental des avancées futures en photonique ultrarapide.

Table of Contents

LIST OF FIGURES

LIST OF TABLES

LIST OF ABBREVIATIONS AND SYMBOLS

Abbreviations

ALLS	Advanced Laser Light Source
CPA	Chirped Pulse Amplification
CW	Continuous Wave
DFG	Difference Frequency Generation
EMT	Energie Matériaux Télécommunications
EAM	Electro-Absorption Modulator
XPM	Cross-Phase Modulation
eV	Electron Volt
FROG	Frequency Resolved Optical Gating
FWHM	Full-Width Half Maximum
FTL	Fourier Transform-Limited
FS	First Stokes
GDD	Group Delay Dispersion
HCF	Hollow Core Fibers
HHG	High-Harmonic Generation
INRS	Institut National de la Recherche Scientifique (French)
LASER	Light Amplification by Stimulated Emission of Radiation
MEMS	Microelectromechanical systems

OPO	Optical Parametric Oscillation
OPA	Optical Parametric Amplifier
PG-FROG	Polarization-Gate FROG
RMS	Root Mean Square
RI	Refractive index
SFG	Sum Frequency Generation
SHG	Second Harmonic Generation
SS	Second Stokes
SPM	Self-Phase Modulation
SF	Short Pass Filter
SD FROG	Self-Diffraction FROG
SRS	Stimulated Raman scattering
THG	Third Harmonic Generation
TDM	Time-division multiplexing
TADPOLE	Temporal Analysis by Dispersing a Pair of Light E-fields
LP	Long Pass Filter
LD	Laser diode
WDM	Wavelength Division Multiplexing

Chemicals

BaB_2O_4	Barium borate (Crystal)
CH_4	Methane (Gas)
CO_2	Carbon Dioxide
Ti:Sa	Titanium Saphire
Ti^{3+}	Titanium ion in the +3-oxidation state
He-Ne	Helium-Neon
N_2	Nitrogen (Gas)
Nd^{3+}	Neodymium ion in the +3-oxidation state
Yb^{3+}	Ytterbium ion in the +3-oxidation state
YAG	Yttrium Aluminum Garnet
YLF	Yttrium Aluminum Fluoride
ZnSe	Zinc Selenide (Crystal)

Units

m	Meter
mm	Millimeter (10^{-3}Meter)
μm	Micrometer (10^{-6}Meter)
nm	Nanometer (10^{-9} Meter)
J	Joule
mJ	Millijoule (10^{-3}Joule)
μJ	Microjoule (10^{-6} Joule)
nJ	Nanojoule (10^{-9} Joule)
KHz	Kilohertz (10^{3} Hertz)
MHz	Megahertz (10^{6} Hertz)
s	Second
ns	Nanosecond (10^{-9}Second)
ps	Picosecond (10^{-12}Second)
fs	Femtosecond (10^{-15}Second)
W	Watt
mW	Milliwatt (10^{3}Watt)
GW	Gigawatt (10^{9} Watt)
TW	Terrawatt (10^{12} Watt)

Notations

c	Speed of Light
f	Frequency of Light
I(t)	Intensity
k	Wave Number
M	Magnification
n	Refractive Index
n_2	Nonlinear Refractive Index
AC	Autocorrelation
S(ω)	Spectrum
ϕ(ω)	Spectral phase
Φ	Phase
λ	Wavelength
τ	Pulse Duration
ω	Angular Frequency
χ	Susceptibility
Δv	Frequency-Domain Width
Δt	Time-Domain Width
$\propto$	Proportional
D	Dispersion parameter
ε_0	Vacuum permittivity
χ (j)	J^{th} order susceptibility

1 INTRODUCTION

1.1 Introduction of Ultrashort Pulse Laser

Ultrashort laser pulses are extremely small amounts of electromagnetic radiation, usually in the range of a few picoseconds (10^{-12}seconds), less than the thermal vibration period of molecules, first attained in the 1960s [1] using the mode-locking approach [2]. Soon after lasers were developed, pulses spanning just a few picoseconds were generated using pulse-generating techniques and dye lasers with broad emission ranges, resulting in reduced pulse lengths to hundreds of femtoseconds (10^{-15} seconds) by the 1970s [19]. Using dye lasers, even shorter pulses, sub-10 femtoseconds, were produced in the 1980s [20]. But early in the 1990s, the Titanium Sapphire Kerr-lens mode-locked laser [5] and the Chirped Pulse Amplification (CPA) [6] technology made these more useful by using the Kerr effect and the wide emission spectrum [21] of the Titanium Sapphire (Ti: Sapphire) laser combined with diode-pumped solid-state lasers, which simplified ultrashort pulse creation and rapidly replaced dye lasers. The CPA method [7] developed in 1985, transformed the discipline by allowing the development of high-intensity ultrashort pulses in solid-state laser systems. CPA operates first in a primary laser oscillator, creating low-energy ultrashort pulses. These pulses are broadened in time by chirping their frequency (to lower intensity and prevent component damage), then amplified, and lastly compressed back to their original duration for usage in many applications. Compared to previous systems, this approach generated ultrashort pulse lasers more affordable, stable, and accessible. In order to pulse stretching and compression, CPA first used diffraction gratings, but more recently, chirped mirrors [22], fiber stretchers, and prism or grism compressors [23] have become popular. These developments have improved ultrashort pulse laser usefulness and efficiency even further [24].

1.2 Historical Background of Lasers

Albert Einstein's 1916 [25] theory that photons may generate similar photons from excited atoms to be emitted set the first conceptual basis for the laser. In 1928, Rudolf Ladenburg indirectly presented evidence of stimulated emission. However, at that time, physicists classified the phenomena as "negative absorption" and judged it to have little bearing on anything. This rejection resulted from the general belief that Boltzmann population distributions dominate, with higher energy states naturally less than lower levels. In 1940, the Russian physicist Valentin A. Fabrikant suggested that under suitable conditions, stimulated emission inside a gas discharge might amplify light emitted. Willis Lamb, Jr. and R. C. Rutherford noted in World War II that population inversions may be produced via nuclear magnetic resonance. Using this mechanism, Edward M. Purcell and Robert V. Pound then found 50 kHz radio wave stimulated emission

[25]. Charles H. Townes enhanced the conceptual progress in 1951 by suggesting that stimulated emission at microwave frequencies can oscillate inside a resonant cavity, producing coherent output. Then, in 1954, Townes and his pupil James Gordon showed the first microwave "MASER," which stands for microwave amplification by stimulated emission of radiation. They tuned excited ammonia molecules into a resonant cavity where they oscillated at 24 GHz [25]. In 1960, Theodore Maiman [25] invented the first ruby LASER, standing for light amplification by stimulated emission of radiation; the prototype of the fiber laser also came from the same era. Optical fiber technology emerged in the 1980s and drove quick developments in fiber laser technology. The development of fiber connectivity and other uses in the 1990s has driven ultrafast fiber lasers front stage as a major research priority. In the field of optoelectronics research, their clear benefits—small size, great efficiency, energy economy, and stability—make them a top tool [25]. Figure 1-1 shows several objects and events set on logarithmic time scales. Our perceptual capacity identifies motions spanning periods longer than about 100 milliseconds (ms). For a filmstrip, for example, it is considered a continuous sequence even if each frame has usually 20-millisecond delay [26]. Mechanical shutters, which control exposure duration in photography, typically operate with a latency of approximately 1 millisecond. Object motion exceeding this exposure duration causes motion blur, leading to an indistinct image. However, strobes allow exposure lengths as short as 1 microsecond (1 μs), which lets us capture events like a bullet in flight. Short bursts of light emitted by stroboscopes allow viewers to see fast-moving phenomena as a sequence of stationary images instead of a continuous blur [26]. A sequence of photos via an open shutter at a slower pace by timing strobe flashes with fast motion, like that of a turbine rotor, can be obtained. The sampling rate, which theoretically can be adjusted quite low, is determined by the frequency difference between strobe flashes and the rapid repeating motion. This method, originally developed by H.E. Edgerton at MIT, can also be used to record a single ultra-high-speed picture [26].

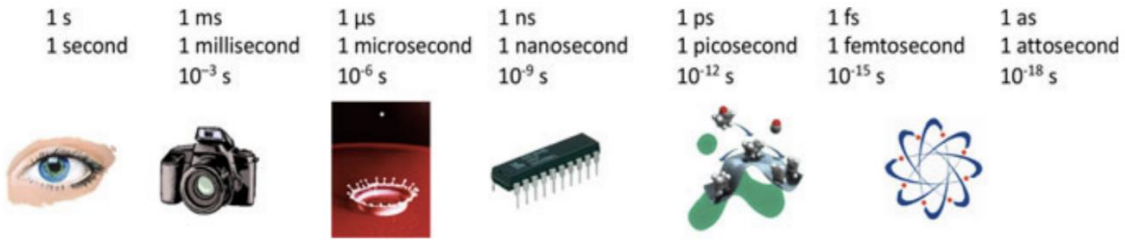

Figure 1-1 **- Time scales over 18 orders of magnitude. Adapted from [26], page 26.**

Molecular vibration is the periodic motion of atoms relative to each other under preservation of the center of mass of the molecule. Usually occurring within durations between 100 and 10 femtoseconds (fs), molecular vibration corresponds to vibrational frequencies between 10 and 100 Terahertz (THz). Especially, chemical reactions can occur at a hundred-fs timescale [11]. Using ultrashort laser pulses, femto-chemistry allows us to examine these processes on their natural timescales, a feat acknowledged with a Nobel Prize in Chemistry in 1999 [26]. Attosecond resolution is essential for exploring electron dynamics in molecular structures before electrons transition to the moving atomic arrangement. Attosecond science has enabled the precise quantification of ionization dynamics, including tunneling ionization, multiphoton ionization, and high-energy single-photon ionization. Ultrafast laser physics enables the investigation of temporal processes spanning 18 orders of magnitude—from seconds to attoseconds—within a laboratory-scale setup, all conducted on an optical table [26].

Short-time spectroscopy with ultrashort laser pulses allows us to track fast events in technology and nature. Usually, this is achieved through pump-probe measurements, in which a delayed probing pulse investigates the changes over time while a strong pump pulse initiates a rapid process. These two pulses are synchronized, ideally coming from the same laser source, which allows femtosecond delays to be introduced between them using a simple mechanical delay line. This arrangement enables precise variation of the laser pulse timing difference, where a delay of 1 femtosecond corresponds to an optical path length difference of approximately 0.3 micrometers. With sub-nanometer accuracy, piezometers may further fine-tune the optical path length, hence allowing delay control with resolutions down to a few attoseconds. A major constraint in resolving ultrafast dynamics is often imposed by the finite durations of the pump and probe pulses, which are typically at least an order of magnitude longer than the process timescales of interest. The ultrafast laser pulse repetition rate is calculated from the time it takes the pulses to complete a round-trip inside the laser cavity. Only a fraction of each pulse reaches the output coupler, from which it is partially transmitted out of the system. Therefore, a sequence of pulses with a frequency matching the frequency of the pulses moving inside the cavity can be obtained. A three-millimeter linear cavity, for example, would produce a 50 Gigahertz (GHz) pulse repetition rate. Using a single carrier frequency, long-distance optical communication nowadays usually runs at a pulse repetition rate between 5 and 10 GHz. Clock speeds in computers have steadily increased; average home computers today have clock rates above 1 GHz. Light pulses are expected to play a central role in future high-speed interconnects, positioning them as critical components in next-generation computing architectures [26].

1.3 Comparison of Titanium: Sapphire and Ytterbium-Based Lasers

High-power ultrafast solid-state lasers, such as those using tiny rods of Titanium-doped Sapphire as the amplification medium, have significant benefits with their greater pulse energies, more power, and shorter pulse durations than dye lasers. Scaling average power is challenging in these systems since low-efficiency direct diode pumping is not feasible. Moreover, limiting their usage in industrial surroundings is the complexity of short-pulse, high-energy Ti: Sapphire lasers [12].

The Ti: Sapphire laser is renowned for its broad gain bandwidth—usually ranging from 650 nm to 1100 nm— and is ideal for applications requiring precision control over pulse characteristics and excellent temporal resolution. This wide bandwidth is necessary for generating ultrashort pulses and can also help generate pulses as short as ten femtoseconds. On the other hand, Ytterbium-doped lasers—like fiber lasers—typically have a lower gain bandwidth, targeted on 1030 nm. Although their gain bandwidth is narrower, Ytterbium-based lasers offer several advantages, including improved thermal management, higher efficiency, and potentially greater average power output. These features make Ytterbium-doped lasers suitable for industrial applications where durability and power efficiency are the most important factors [4].

1.4 Motivation

Nonlinear optical processes such as Optical Parametric Amplification (OPA)[10], Optical Parametric Generation (OPG), and Difference Frequency Generation (DFG) are commonly used to gain a broader spectral range from a given wavelength [10]. All these techniques require a solid-state nonlinear crystal and interaction between two or more optical waves, which are particularly effective for generating longer wavelengths. Our goal is to achieve longer wavelength sources. On the other hand, solid-core optical fibers made from silica-based materials lack energy scalability due to their low damage threshold, resulting in limited frequency shifts. An alternative method is to involve vibrational SRS using gases as a nonlinear medium, which enables access to larger vibrational frequency shifts. For instance, Hydrogen has the largest shift, but the rotational effect can interfere with the vibrational SRS [27]. However, CH_4 is a symmetric top molecule and does not show the rotational Raman signal, making it a promising nonlinear medium for the vibrational SRS effect. The motivation of this study is to develop high-energy, frequency-shifted light sources based on vibrational SRS in CH_4.

1.5 Structure of Thesis

Chapter 1 introduces the field of ultrashort high-power lasers and outlines the motivation of the study. Chapter 2 explains the basic operating principle of a laser and the mechanism behind the generation of ultrashort pulses. Chapter 3 is dedicated to an introduction of key concepts in nonlinear optics, while Chapter 4 discusses the different experimental methods used to characterize ultrashort laser pulses, focusing on FROG as well as the required numerical tool to retrieve pulse properties. Chapter 5 presents the specific experimental setup employed in this MSc thesis and the results of the experiment. Chapter 6, Finally, summarizes the main conclusion of the work.

2 FUNDAMENTALS OF ULTRASHORT LASER PULSES

2.1 Basic Principles of Lasers

A laser is a device that generates extremely directional electromagnetic (EM) radiation. This radiation is visible light in the visible region. However, lasers can emit radiation beyond the EM spectrum—all this radiation is called "light" for short. The abbreviated version "laser", derived from the acronym "light amplification by stimulated emission of radiation", emphasizes its operating mechanism [28]. Lasers work by stimulated radiation emission. Figure 2-1 shows a basic four-level laser configuration. Although there are other energy level structures, such as the three-level laser, which change depending on the type of laser, the fundamental ideas of laser operation remain constant among all laser kinds. Four separate energy levels form the system shown in Figure 2-1. Beginning at ground level (1), the system is stimulated to level 4, usually by optical means using photons with energy $\hbar\omega_{pump}$ supplied by a flashlamp or similar laser, sometimes referred to as a pump laser. Level 4 is shown as a broad band of levels instead of a single level, which is common in real systems [28]. The population then rapidly relaxes from level 4 (the excitation level) to the upper lasing level (level 3). Laser activity occurs on the level 3 to level 2 transition and depends on a population inversion between levels 2 and 3. Population inversion, often referred to as a non-Boltzmann distribution, occurs when the upper energy level (level 3) has a higher population than the lower level (level 2) [28]. Achieving population inversion requires maintaining a low population in level 2 while ensuring a high population in level 3. This is obtained by exciting from level 1 to level 4, then fast relaxation into level 3. Level 3 is considered optically pumped when its population is sufficiently increased to achieve population inversion. The energy difference between level 3 and level 2 defines the frequency (or color) of the laser radiation. Stimulated emission from level 3 to level 2 results in the coherent output at this characteristic frequency. Another quick population migration from level 2 back to the ground state guarantees that the population of the lower lasing level stays low, hence allowing the preservation of a notable population inversion for effective lasing [28].

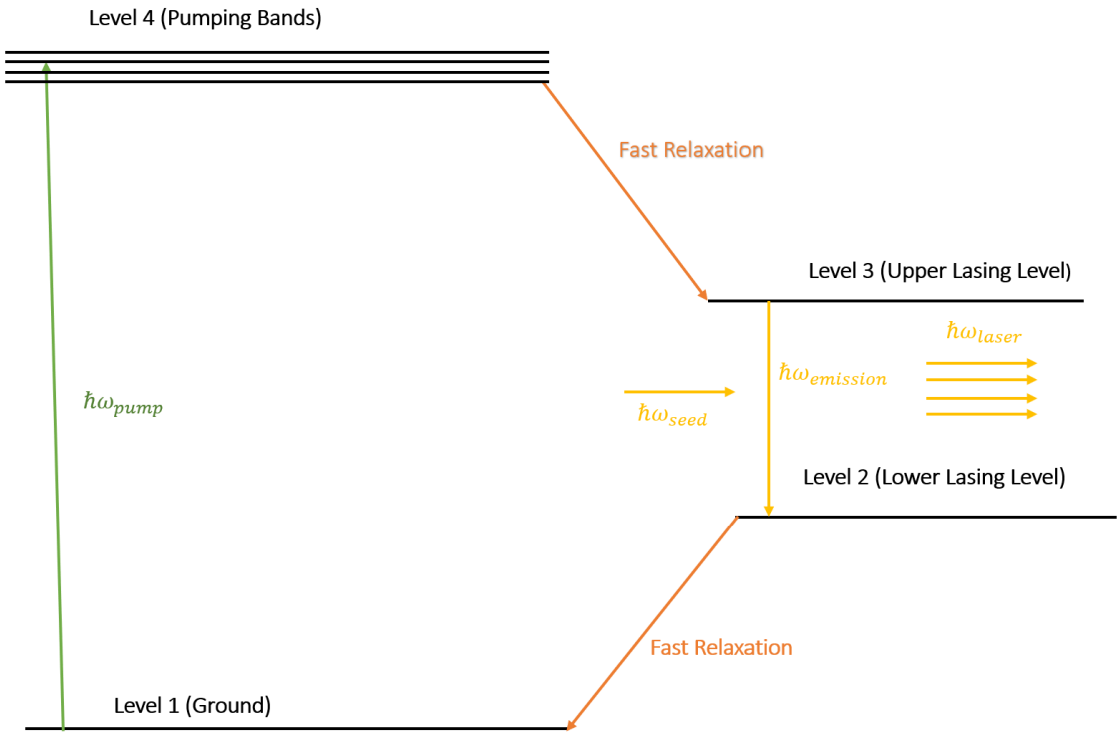

***Figure 2-1*- A schematic of basic laser action. Lasing is achieved between levels 2 and 3, via excitation from level 1 to level 4. Reproduced with permission from [28], page 1-2.**

Levels 2 and 3 can correspond to broader energy bands, enabling a wider lasing bandwidth. This broader bandwidth is essential for generating ultrashort laser pulses. The given pump and emission energies have been chosen for demonstrative purposes. The Ti: Sapphire laser has a broader emission bandwidth among other solid-state lasers, which makes it ideal for generating ultrashort pulses. It is usually pumped at around 527 nm and produces emission between 700 nm and 900 nm. Doped into many media, including YAG (producing Yb: YAG lasers), Yb^{3+} ions enable ultrafast lasers, and Yb-doped fiber lasers are becoming common in optical laboratories around the world [28].

The gain medium or laser medium is the substance in which the lasing process occurs. There are wide variety of laser media available, including gases, liquids, and solids. Solid-state laser media are the most commonly used in the field of ultrafast lasers. These lasers operate based on an active ion doped into a solid host material. This ion is doped into a host glass or crystal where the laser operation is determined by the energy levels of the ion within this crystal field. Common active ions are Nd^{3+}, Ti^{3+}, and Yb^{3+} which can be doped into different hosts to provide diverse laser actions. Following the conventional

nomination of ion: host, Table 2-1 shows instances of lasing systems attainable with these active ions doped into common hosts. For Nd^{3+} ions, for example, YAG (Yttrium Aluminum Garnet) and YLF (Yttrium Aluminum Fluoride) are often hosts. Table 2-1 shows how small changes in the chemical structure of the host can be used to control the emission energy [28].

Table 2-1 Common solid-state laser media and their characteristic lasing energies. Adapted from [4].

Laser Medium	Pump Energy wavelength [nm]	Emission Energy wavelength [nm]
Ti-Sapphire	400-600	650-1100
Nd: YAG	730-820	1064
Nd:YLF	730-820	1053
Yb: Fibre	940	1020-1040

2.2 Pulse Generation

The aforementioned media can be configured to operate either as laser amplifiers or as laser oscillators, depending on the optical feedback and system design [26].

2.2.1 Amplifiers

A laser amplifier is an essential component of a laser system, which increases the power level of an already-existing laser beam to a target level. Though they have different geometries and traits, several geometries of laser amplifiers have some characteristics in common. Within ultrafast optics, amplification usually consists of a laser medium, a pump laser, and a smaller seed laser. The seed laser beam is amplified by absorbing energy that has been transferred from the pump laser to the laser medium. The amplifier reduces the energy of the pump beam while raising the energy of the seed beam. Figure 2-2 shows a simplified schematic of the amplification process. The laser medium is sometimes referred to as a gain medium. Although these words are interchangeable, gain medium is more commonly used when referring especially to amplifiers [26]. The gain of the amplifier is the degree to which the energy of the seed beam is increased; usually stated as the ratio of the output power to the input power. Usually functioning within a given frequency range, laser amplifiers are limited by the finite emission bandwidth of the gain medium.

The gain bandwidth is the range of effective amplification. A broad gain bandwidth is essential in ultrafast laser systems to ensure efficient amplification across the full spectral width of ultrashort pulses. But when the amplifier cannot increase the whole bandwidth of the input pulse, gain narrowing—a decrease in the bandwidth of the pulse after amplification—results. Depending on the degree of gain generated, laser systems might feature several amplification stages—mostly classified as preamplifiers and power amplifiers [28].

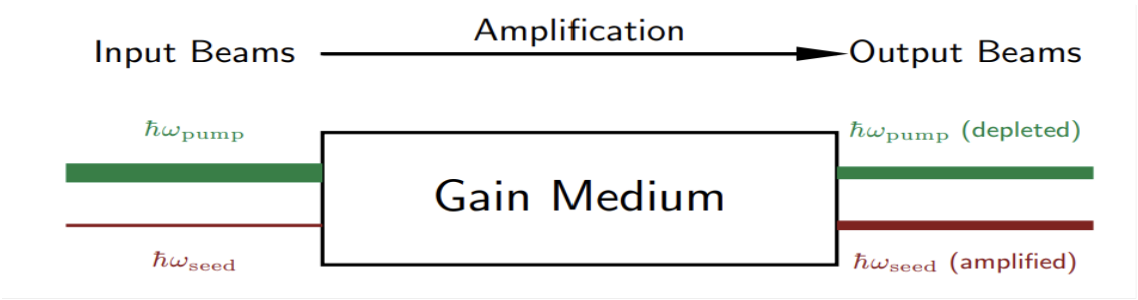

***Figure 2-2*- Simplified schematic of how a laser amplifier works. The incoming seed beam (red) is amplified, and the pump beam (green) is weakened via interaction in the gain medium. Adapted from [28], page 1-5.**

2.2.2 Oscillator

A laser oscillator is an essential component in producing the first weak laser pulses. Basically, these weak pulses are employed as a seed for amplification of the laser system. In a simple sense, feedback to a laser amplifier—sending some of the amplified output back to the amplifier input—causes oscillation at the frequency of the light given back. This approach generates more of the same stimulated emission by guiding the output light from a stimulated emission process back into the input. Oscillation is accomplished by building an optical cavity around an amplifier. In each process, the laser beam passes through the gain medium via this cavity, which allows it to resonate inside the cavity. The cavity then guides the emitted light back to the input, therefore triggering more emission and oscillation. An optical cavity is a closed gap between mirrors, whereby a laser beam transferred into it bounces back and forth instead of running straight through. A condensed schematic showing how an amplifier might be turned into an oscillator is given in Figure 2-3 [28].

The function of the oscillator in Figure 2-3 is described as follows. Circled number (1) shows emission, which is generally stimulated from the gain medium and is directed into the cavity using mirrors. Circled number (2) represents the emission traveling around the cavity. It is directed back into the gain medium, making subsequent stimulated emission and oscillation. Circled number (3) demonstrates the first mirror

after the gain medium, which is an output coupler, a partially reflective mirror that reflects some light into the oscillator (as in step (1)). However, it allows some light to get amplified further in the laser system. It is crucial to ensure that the oscillator is oscillating in the desired way to produce the pulses you want is a key design consideration. There are often multiple competing processes occurring within the oscillator cavity, producing various kinds of laser output. There is a certain amount of gain and loss while the light makes one complete circuit around the cavity. If the round-trip gain is larger than the cavity loss, then the laser will generate output. On the contrary, if the cavity loss is larger than the round-trip gain, then there will not be any laser output. The key point at which the round-trip gain overcomes the cavity loss is referred to as the lasing threshold. The design and alignment of the oscillator need to be such that the desired process has the highest round-trip gain and lowest losses, so that it predominates over other unwanted processes *[28].*

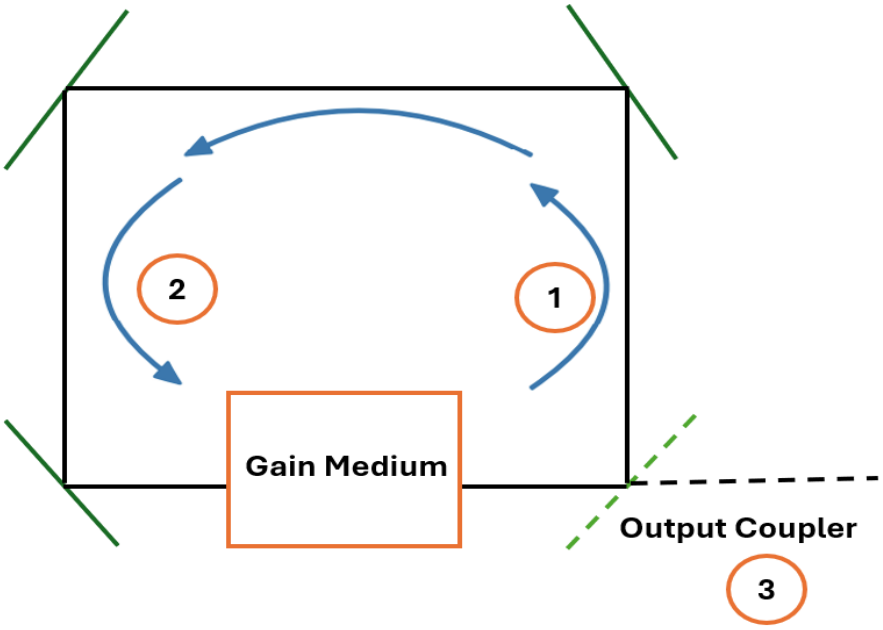

***Figure 2-3*- A simplified diagram of a laser oscillator: Laser beams within the cavity, formed by green mirrors, are depicted in black, while the direction of their movement around the cavity is illustrated by blue arrows. Key areas of the cavity are highlighted with circled numbers. It is important to note that the diagram does not include the oscillator pump beam. Reproduced with permission from [28], page 1-6.**

Laser sources can be divided mostly into pulsed lasers and continuous wave (CW) lasers, depending on their mode of operation. Gas lasers (like He-Ne or CO_2), semiconductor lasers (like Nd: YAG or Ti: Sapphire), and dye lasers—which comprise solutions like Rhodamine or Malachite green—can all be used with these lasers across different systems. CW lasers typically exhibit narrow spectral bandwidths. A fast optical

shutter can be implemented at the output to generate laser pulses from a CW laser. This can be achieved, for example, by incorporating a Pockels cell and a linear polarizer inside the laser cavity. This arrangement allows for the generation of temporal widths ranging from 10 to 100 nanoseconds $(10^{-9}\,s)$ for laser pulses. Applying the suitable voltage across the Pockels cell acts as a waveplate, changing the polarization of light flowing through it from 's' to 'p,' subsequently the linear polarizer rejects it. This approach, sometimes known as active switching, is constrained in speed by the highest possible speeds of electronic switching devices [29]. For those using ultrashort pulses, the main difficulty is finding a suitable laser capable of producing radiation at the target wavelength. Although this method provides broad and convenient coverage for the visible spectrum, reaching the infrared spectrum proved more problematic due to the lack of suitable dyes and the related problems like toxicity and poor photochemical stability of existing choices. Cryogenic color-center lasers allowed tuned ultrashort pulses within the near infrared spectrum [11]. After selecting a suitable laser, ultrashort pulses can be generated using the mode-locking technique. Fiber lasers typically generate ultrashort pulses through various pulse formation mechanisms. While mode-locking can reach femtosecond-level pulse widths, Q-switching generates nanosecond-width pulses. Active and passive modes of locking exist for this process. Whereas passive mode-locking uses intra-cavity mode-locked devices to produce ultrashort pulses, active mode-locking modulates resonant cavity parameters via an external periodic signal. One commonly used technique is integrating a saturable absorber into the laser cavity and using its nonlinear absorption characteristics. This procedure dissipates the low-intensity ends and preserves the core high-intensity section, resulting in a narrower pulse. Artificial, based on fiber nonlinear interference effects, and real, using the nonlinear saturable absorption characteristics of materials, are the two types of saturable absorbers. Passive mode-locking is essential for generating femtosecond pulses, making the study and optimization of passively mode-locked fiber lasers a subject of considerable research interest [11].

These methods require some types of amplitude modulation given to the laser radiation using a period relative to the cavity round-trip duration, either externally derived—as in the case of active mode-locking—or passively acquired from the radiation itself employing an intensity-dependent loss process. Gain-switching, another approach for ultrashort pulse creation, generates femtosecond pulses by pumping a sequence of short cavity lasers with ever-shorter pump pulses. This method is especially successful with dye lasers using UV excimer pump lasers, therefore allowing extensive spectral coverage. Despite this, CW lasers are commonly preferred in experimental setups, as they enable the generation of shorter and cleaner pulses. Pulse shaping occurs gradually over multiple cavity round-trip. Passively mode-

locked CW lasers provide ultrafast signals with large peak-to-background intensity ratios. The mode-locking method used depends on elements including the characteristics of the laser media, required pulse duration, pragmatic concerns, including cost and stability, pulse quality criteria, and the need to synchronize with other signals [29]. After specifying the desired pulse duration and central wavelength, determining the necessary gain bandwidth becomes a critical design factor. According to the uncertainty principle, an ultrashort pulse in the time domain necessitates a broad spectral width in the frequency domain. Thus, it is critical to make sure the gain medium has a suitably large bandwidth to efficiently amplify the ultrashort pulses. From energy-time uncertainty $\Delta E \times \Delta t \geq \frac{h}{2\pi}$ Time-Bandwidth Product (TBP) with zero chirp Gaussian profile can be obtained using this formula: $\Delta\tau_p \times \Delta\omega_s \geq 0.441$ [30].

2.3 Chirped Pulse Amplification

The shortest ultrashort pulses can reach durations of just a few attoseconds (1 as = 10^{-18} seconds). Early 2000s research by Paul Corkum and Ferenc Krausz [3] is usually credited with producing attosecond pulses in a pioneering manner. Their development of high-order harmonic generation (HHG) in gases resulted in attosecond pulses, which have helped to examine faster time-scale physical processes and to design and investigate exotic nonlinear optical features, including optical beam filamentation [3, 4].

Due to their extremely short durations, these pulses can reach high peak intensities (~10^{12} W/cm²) while maintaining low average powers, making them ideal for investigating phenomena that occur on ultrafast timescales. Pulse duration has been shortened to the level of hundreds of femtoseconds 10^{-15} thanks to developments in pulse generating methods, including the use of large dye lasers with broad emission bandwidths, Ti: Sapphire Kerr-Lens mode-locked laser, as well as the CPA technique [6]. The development of ultrashort laser pulses is depicted below [31].

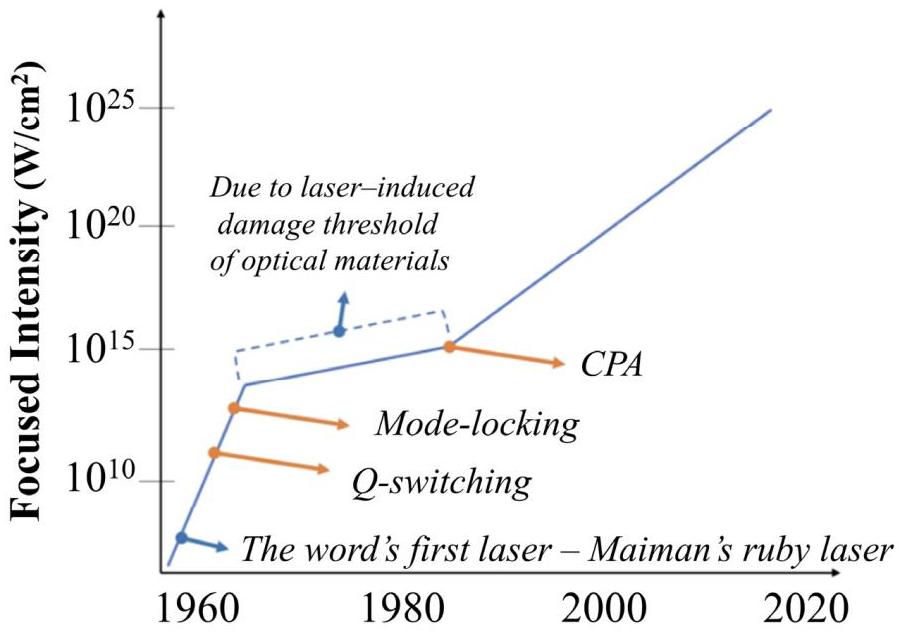

Figure 2-4: **History of laser intensity. Adapted from [32].**

The concept of CPA, introduced by Donna Strickland in 1985, is fundamental to the generation of high-intensity, ultrashort laser pulses [6]. This technique has driven Ti: Sapphire laser technology to the point where producing multi-millijoule, sub-50 fs pulses is now a routine practice [8]. Since self-focusing limits the amplification of ultrashort laser pulses, CPA was developed to overcome the critical limitation of optical damage and nonlinear distortion that arises when amplifying femtosecond pulses directly. Due to their extremely short duration, such pulses possess extremely high peak powers even at modest energy levels. When amplified without modification, these intense pulses can cause self-focusing, SPM, and even physical damage to optical components or gain media. This fundamentally limited the ability to scale pulse energies for applications requiring high peak power. CPA addresses this issue through a three-step process: stretching, amplifying, and compressing the pulse. Firstly, the pulse is stretched using a positively dispersive delay element before amplification. Then, a negatively dispersive delay element compresses the pulse back to its starting pulse shape [6]. A short, low-energy pulse is deliberately stretched using a pulse stretcher—in this case, by propagation through a single-mode optical fiber—to produce a temporally stretched pulse. Within the fiber, the pulse undergoes linear chirping due to a combination of SPM and group velocity dispersion (GVD). Once stretched, the pulse can be amplified to significantly higher energy levels than would be possible in its original, unmodified form. This stretching step is crucial, as it enables energy scaling without reaching the self-focusing threshold, since the peak intensity remains low during

amplification. Following this matter, a grating pair compresses the stretched pulse after amplification. Higher energy levels before self-focusing are obtained by increasing the stretched pulse instead of the compressed one. This amplification mechanism appears not to affect the linearity of chirping, therefore allowing total pulse compression. Amplifying a chirped pulse in a non-uniform medium has another benefit in terms of the gain sweeping phenomenon [6]. The following images depict the chirped pulse amplification schematic method.

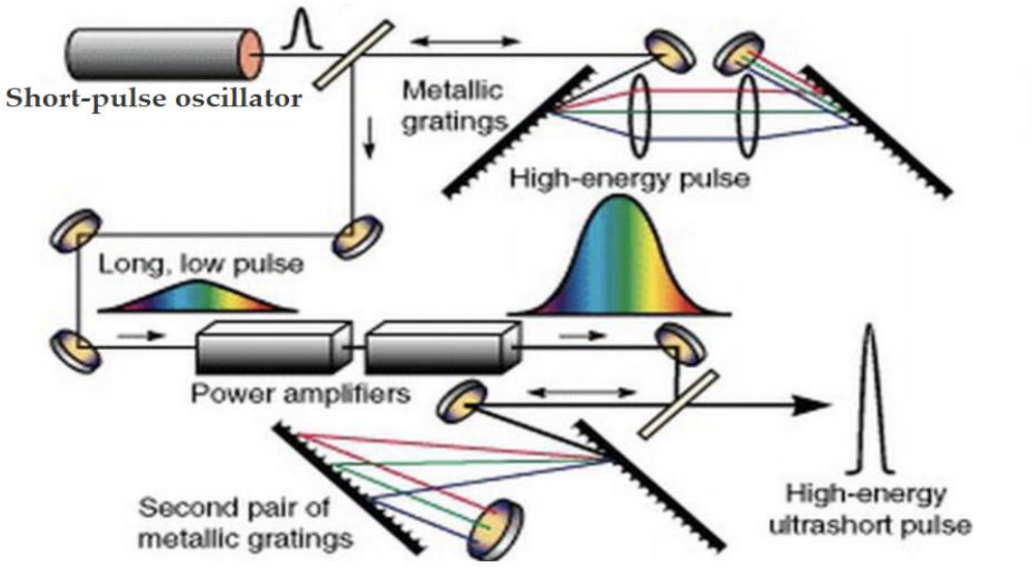

Figure 2-5: **Schematic of the CPA technique. An ultrashort pulse is stretched, amplified to high energy, and then recompressed to produce a high-energy ultrashort pulse. Adapted from [30].**

2.4 Applications of high-energy ultrashort pulses

The high temporal resolution of ultrafast pulse lasers makes them highly desirable for time-resolved applications. Measuring techniques and conventional lasers are not responsive to rapid transient events. Ultrafast lasers let researchers explore and measure phenomena occurring on short times using femtosecond and picosecond pulse lengths. In fields such as chemistry, where understanding of the kinetics of molecular interactions and chemical processes is basic, this capacity is extremely crucial [33]. For example, femtosecond laser pulses have been observed during the transition phases of chemical reactions, therefore providing knowledge on molecular interaction and chemical reaction mechanisms and pathways. Ahmed Zewail, who received the 1999 Nobel Prize in Chemistry, invented the field of femto-

chemistry by looking at the transition states of molecules during chemical reactions using femtosecond spectroscopy [33].

Ultrashort pulse lasers can reach quite high peak intensities since they concentrate energy into very short pulses. Longer pulse duration or CW lasers cannot generate nonlinear optical phenomena, as these high intensities are sufficient to produce them. Nonlinear optics forms the foundation of several complex technologies, including harmonic generation, multiphoton excitation microscopy, and the generation of new light frequencies. Nonlinear processes, including second-harmonic generation (SHG) and third-harmonic generation (THG), for instance, result from ultrafast pulses interacting with materials. SHG and THG from visible or infrared laser sources can double or triple the frequency of the incident light, respectively. Simultaneous absorption of two or more photons to excite a fluorophore allows multiphoton excitation microscopy to produce deep-tissue imaging with minimum photodamage and outstanding resolution, so changing biological imaging [34].

In industrial applications, ultrashort pulse lasers offer a significant reduction in thermal damage. These pulses can also ablate low-thermal diffusion materials, thereby enabling precise micromachining of delicate objects. Especially in the medical device and electronics industries, this function is helpful. For example, femtosecond laser micromachining generates sub-micron accuracy complex forms in materials including glass, polymers, and metals. This approach is for the fabrication of optical waveguides, biomedical implants, and microelectromechanical systems (MEMS). The lack of significant heat effects ensures that the material properties remain unaffected, and the accuracy of the ablation process enables the fabrication of complex three-dimensional features [3].

The telecommunications industry also takes advantage of ultrashort pulse lasers. These lasers allow high-speed optical communication systems by offering data transfer speeds orders of magnitude quicker than those of conventional electrical systems. Due to their ability to enable rapid switching and modulation, ultrafast lasers have significant applications in optical signal processing. For example, optical fiber communication systems utilize ultrashort pulses to transmit data over long distances, owing to their minimal dispersion and low transmission loss. Techniques such as time-division multiplexing (TDM) and wavelength-division multiplexing (WDM) achieve large data throughput through precise control of ultrafast pulse timing and wavelength allocation [35]. Moreover, frequency combs are generated by ultrafast pulse lasers with accurate optical rulers employed in spectroscopy and metrology [35].

Recent advances in ultrafast optics have enabled the generation of optical pulses with durations reaching into the attosecond (10^{-18} seconds) regime. HHG techniques produce high-order harmonics using nonlinear interactions between a femtosecond laser pulse and a gas medium, therefore generating attosecond pulses. Attosecond pulses generate unprecedented benefits in science and quantum physics by letting scientists see and manipulate electronic processes inside atoms and molecules [3].

Mid-infrared ultrashort pulse lasers have a wide range of applications, particularly in medical diagnostics, material processing, molecular spectroscopy, and chemical synthesis. Mid-infrared (mid-IR) lasers, due to their high sensitivity to vibrational modes, enable detailed probing of molecular dynamics and structures [36, 37].

3 NONLINEAR INTERACTIONS OF LIGHT IN OPTICAL MEDIA

3.1 Nonlinear Propagation Principles

In nonlinear optics (NLO), the behavior of light in nonlinear media, where the polarization density "P" shows a nonlinear response to the electric field "E" of the light is studied. This nonlinear behavior becomes clear at very high light intensities, usually when the electric field of the light exceeds 10^8V/m, therefore reaching values equivalent to the atomic electric field of roughly 10^{11}V/m [10]. Here are several forms of nonlinear optical events capable of extending laser wavelength capability, which arise from the optical behavior of materials under high-intensity light. Unlike conventional lasers, where the medium stores energy in electronic or vibrational states and lasing occurs through transitions between those states, these nonlinear processes, including SRS, OPA, SHG, and DFG, use the medium for interaction between two or more optical waves. HHG is an extreme kind of nonlinearity whereby electrons release radiation under the effect of an incident pump beam [10].

Induced polarization, denoted by "P", is the result of a displacement of the electric charge of molecules and atoms within a substance under the influence of a common light source with an electric field strength (or intensity). "P" and "E" have a linear relationship; the degree of induced polarization is exactly proportional to the amplitude of the electric field [10].

$$\boldsymbol{P} = \varepsilon_0 \chi^1 E^1 \quad (3.1)$$

Where χ^1 is linear susceptibility, a complex number tensor for the anisotropic medium and ε_0 represents the permittivity of vacuum. Because the electric field intensity of ultrashort laser pulses is significantly higher than that of ordinary light, the electric polarization can be expanded as a power series in the electric field amplitude. Consequently, for anisotropic media, the relationship between "P" and "E" is expressed as:

$$\boldsymbol{P} = \varepsilon_0 \chi^1 E^1 + \varepsilon_0 \chi^2 E^2 + \varepsilon_0 \chi^3 E^3 + \cdots \quad (3.2)$$

Where χ^2 and χ^3 are the second and third order nonlinear susceptibilities, respectively. χ^1, χ^2, χ^3 are second, third, and fourth rank tensors. "P" and "E" are the vector quantities showing polarization and electric field, respectively [10].

3.1.1 Nonlinear Response of Medium to the Optical Field

In the case of an isotropic homogeneous medium, in the following equation, only a small number of susceptibility tensor elements are nonvanishing and "P" and "E" are the vector quantities; so, the equation can be written as follows:

$$\boldsymbol{P} = \varepsilon_0 \chi^{(1)} \boldsymbol{E} + \varepsilon_0 \chi^{(2)} |E| \boldsymbol{E} + \varepsilon_0 \chi^{(3)} |E|^2 \boldsymbol{E} + \cdots = P^{(1)} + P^{(2)} + P^{(3)} + \cdots \quad (3.3)$$

Where, $P^{(1)} = \varepsilon_0 \chi^{(1)} E$, $P^{(2)} = \varepsilon_0 \chi^{(2)} |E| E$ and $P^{(3)} = \varepsilon_0 \chi^{(3)} |E|^2 E$. While $P^{(1)}$ is the linear polarization, $P^{(2)}$ shows second-order nonlinear polarization and $P^{(3)}$ represents third-order nonlinear polarization. Regarding linear polarization, the polarization of the material corresponds with the electric field strength. On the other hand, for the second and third-order nonlinear polarizations, the polarization of the medium is respectively proportional to the square and cube of the field strength. Second-order nonlinear optical processes develop from the second term in equation (3.3), more especially from processes defined by $\varepsilon_0 \chi^2 E^2$. These systems produce a field in frequency $\omega_{out} = \omega_m + \omega_n$ in response to applied fields at frequencies ω_m and ω_n which may be either positive or negative [10].

3.2 Kerr Effect and SPM

SPM, which was discovered early in nonlinear optics research [9, 11], is a phenomenon that occurs when an intense optical beam travels through a Kerr medium. Kerr medium is a material in which the refractive index changes in response to the intensity of light passing through it, which causes a phase modulation proportional to its intensity distribution due to their nonlinearity. HCF filled with gas, which was first reported in optical fibers in 1978 [38], as a nonlinear medium, provides an appropriate platform for experimental investigation because it enables significant nonlinear effects free from spatial or thermal changes (details in section 3.4) [31]. Light propagation inside a fiber results in a minute change in the refractive index (RI) of the fiber. When the electromagnetic field of the light interacts with the atoms and molecules in the medium, a phenomenon known as the Kerr Effect occurs. A Fourier transform pair describes inversely connected temporal and frequency domains of a laser pulse. This relationship implies that shorter pulse durations correspond to broader spectral bandwidths. Maximizing the frequency bandwidth will help to produce matching short pulses in time using SPM. SPM generates new frequencies in a broad range [39]. Since the refractive index of glass (RI) changes due to the Kerr effect, the middle part, the trailing edge, and the leading edge are different by a small amount. This variation influences the phase of the light waves forming the pulse, therefore affecting frequency. As seen in Figure 3-1, the frequency spectrum of the pulse thus broadens, with lower frequencies appearing at the leading edge and higher frequencies at the trailing edge. The spectrum of the pulse always broadens over the fiber [39]. At the center of the pulse, the positive chirp created by SPM is observed almost linear, producing a chirp—a slow frequency shift—over the whole pulse period. Usually, the form of the pulse and the first chirp added to the pulse define the spectrum. If the same chirp is present at two separate times, the pulse has the

same instantaneous frequency at both sites. These points essentially show two waves with the same frequencies but different phases, which, depending on their relative phase difference, may interact either constructively or destructively. As a result of such interference, the pulse spectrum shows the distinctive oscillating structure [39, 40]. SPM has initiated extensive research into nonlinear optical phenomena. In the case of an input pulsed beam, SPM time-dependent phase change modifies the optical spectrum. The frequency modulation (chirp) of the pulse electric field shapes this change: SPM induces spectrum broadening if the pulse is initially Fourier-transform limited (FTL) or up-chirped. On the other hand, SPM causes spectral compression in an initially down-chirped pulse [38, 41]. Under conditions of strong SPM, the optical spectrum may show notable oscillation.

When an electric field "E" is introduced into a transparent dielectric medium, it distorts the distribution of electron charges within the medium. This distortion leads to an induced polarization "P" within the medium, which, under initial approximation, exhibits linearity in response to the applied "E" field. However, under the influence of a strong electric field "E", the polarization response within the applied field may deviate from linearity. [35].

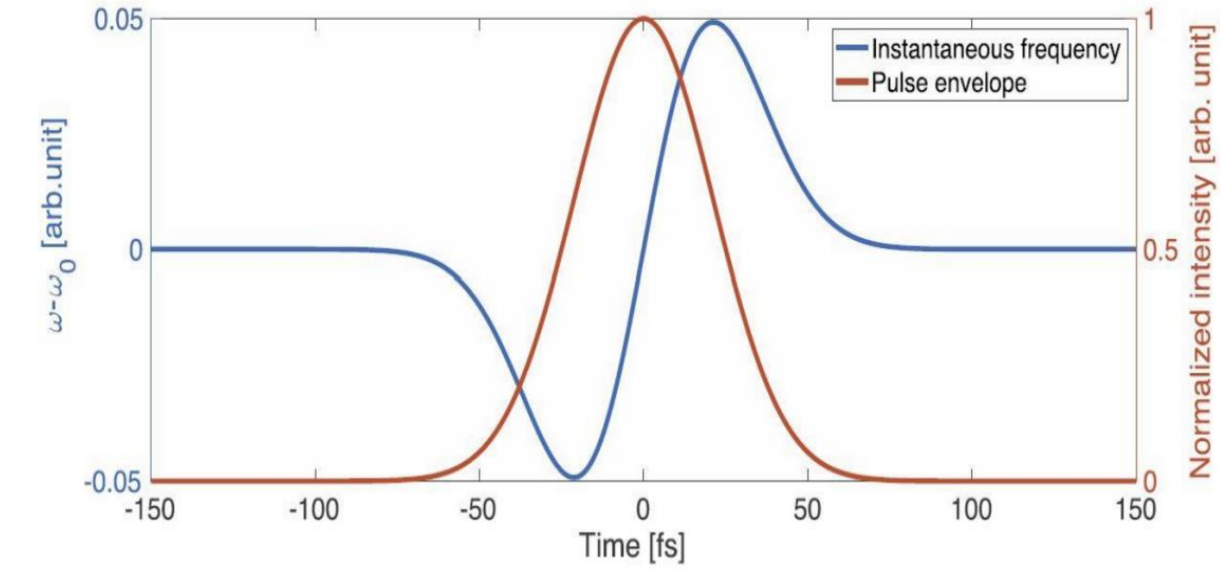

***Figure 3-1*- Illustration of SPM. When an intense ultrashort pulse travels through a nonlinear medium, its time-dependent intensity modifies the refractive index via the optical Kerr effect. This induces a nonlinear phase shift $\phi(t)$, and its time derivative $\frac{d\phi(t)}{dt}$ leads to instantaneous frequency changes across the pulse (represented in blue). As a result, SPM generates spectral broadening, with new frequency components appearing without changing the pulse duration. Adapted from [32].**

Nonlinear phenomena such as SHG and sum frequency generation (SFG) are associated with the second-order susceptibility χ^2. Materials with a Centro-symmetric structure, such as silica fibers, exhibit a zero second-order susceptibility, implying that χ^2 equals zero. As for the third-order susceptibility χ^3, it primarily governs phenomena such as third harmonic generation, nonlinear changes in the refractive index, and four-wave mixing [12].

The third-order nonlinearity induces an intensity-dependent refractive index, which is the principal factor contributing to phase modulation within an individual optical pulse, leading to the generation of SPM. The nonlinear relationship between the refractive index and signal intensity is expressed as: [71]

$$n = n_0 + n_2 I \qquad (3.4)$$

Where n_0 represents the linear refractive index, while n_2 denotes the nonlinear index of refraction. Furthermore, the signal intensity "I", which correlates with the electric field, is represented by:

$$I \propto |E|^2 \qquad (3.5)$$

The nonlinear (intensity-dependent) phase shift of a pulse:

$$\Phi(t) = \frac{\omega}{c} n_2 I(t) L \qquad (3.6)$$

Where "ω" is the angular frequency of the light ($\omega = 2\pi f$) , "c" is the speed of light ($c \approx 3 \times 10^8\ {}^{m}/_{s}$) and "$L$" is the length of the nonlinear medium [12].

SPM, therefore, leads the spectrum of a light pulse to broaden as it passes through an HCF. Figure 3-2 represents an unchirped pulse versus a chirped pulse. Since the radiation intensity is time-dependent, the frequency deviation is likewise time-dependent. Therefore, it can be expressed as: [12]

$$\Delta\omega(t) = \frac{\omega}{c} n_2 L \frac{\partial I}{\partial t} \qquad (3.7)$$

And the spectral broadening can be expressed as: [60]

$$\Delta\omega(t) = \frac{\omega}{c} n_2 L \frac{I_0}{\tau} \qquad (3.8)$$

Where "I"$_0$ shows the peak intensity of the light pulse and "τ" is the pulse duration.

The frequency spectrum following SPM corresponds to the Fourier transform of the pulse amplitude, which is given by: [38]

$$F(\omega) = \frac{1}{2\pi}\int_{-\infty}^{+\infty} P(t)^{1/2} e^{i\Delta\emptyset(t)}\, e^{-i(\omega-\omega_0)t} dt \quad (3.9)$$

The phase shift, denoted as "$\Delta\emptyset(t)$", experienced by the signal "$P(t)$" in a lossless fiber, varies according to both the fiber length "L" and the intensity-dependent refractive index. This refractive index, in turn, correlates directly with the intensity of the signal [38].

$$\Delta\phi(t) = \left(\frac{2\pi L}{\lambda}\right)\delta n \quad (3.10)$$

$$\delta n = \frac{1}{2} n_2 E^2 \ , \ E^2 = 10^7 \left[8\pi \frac{P(t)}{ncA_{eff}}\right] \quad (3.11)$$

Where "n_2" is the nonlinear index in esu units, "λ" stands for the vacuum wavelength, "n" denotes the refractive index, "E" represents the peak field amplitude in cgs units and "$P(t)$" is the pump power in watts [38]. The duration of the pulse is influenced by the mode-locker drive frequency. Tuning this frequency involved maximizing the range of the expanded spectrum using a fast diode and a sampling oscilloscope [42]. This approach proved to be more convenient for optimizing the mode locker compared to the conventional method of assessing the pulse duration using a fast diode and a sampling oscilloscope [38]. SPM is often considered to negatively impact optical communication systems or high-power pulse creation [42]. However, SPM can be a benefit with good management because it drives many types of applications. These benefits comprise the generation of ultra-short pulses [42, 43], compensation of dispersion via soliton effects [44, 45], generation of wavelength-multiplexed sources [31], frequency shifting of ultra-short pulse sources [46], enhancement of contrast for ultra-short pulses [47], various applications in ultrafast optical signal processing [24, 44], the characterization of optical pulses [48, 49], and waveguides [50].

3.3 Stimulated Raman Scattering

There are two types of elastic scattering depending on the scattering particle's size: Mie and Rayleigh scattering [17]. Mie scattering happens when the light of all frequencies is scattered evenly with a particle size that is larger than the incident light, regardless of the wavelength. On the other hand, Rayleigh scattering occurs when the size of the matter is much smaller than the wavelength of the incident light. Depending on the wavelength of the incident light, the difference lies in the degree of scattering. The blue color of the sky results from Rayleigh scattering. Mostly, photons incident on a molecule elastically (Rayleigh scattering) with unchanged wavelength compared to the incident light. However, there is

inelastic scattering in which a few photons scatter in a way that the wavelength of the scattered light is modified as a result of the interaction with a molecule. In 1928, physicist C. V. Raman discovered Raman scattering, which is inelastic scattering [17]. In such a Raman scattering, the wavelength of the light can decrease or increase, which is called Stokes Raman or anti-Stokes Raman scattering, respectively [17]. (See Figure 3-3)

The term SRS describes a collection of optical techniques in which two light fields induce a Raman-active transition in a substance [26]. SRS has been commonly employed since the 1960s to investigate the vibrational properties of gases, liquids, and solids, including those from chemical bonds and groups, which use the same molecular vibrations as spontaneous Raman scattering. This helps to investigate the structural dynamics and interactions of molecules as well as to identify them. SRS generates directional and strong radiation by coherently generating vibrational modes, which are similar but different from the incoherent molecular movements caused by spontaneous Raman scattering. SRS produces far better signal-detecting efficiency than natural Raman scattering. Furthermore, SRS provides direct observation of coherent molecule motions at ultrafast time scales, providing information on processes and molecular dynamics, which are not easily observable via Raman spectra analysis alone. In addition, the strong Raman-sensitive signals and the capacity to resolve molecular motions in time have made SRS a useful instrument in biomolecular imaging, biology, and chemistry [26].

Stimulated light scattering emerges due to a change in the material's optical characteristics caused by the optical field. This induces a nonlinear relation between different components of the field through some form of excitation within the material, leading to modifications in its optical properties. This nonlinearity is typically characterized by a complex susceptibility and a third-order nonlinear polarization concerning the interacting fields. Different forms of stimulated scattering can be explained, but we focus on discussing the two most frequently observed processes, Stokes and Anti-Stokes, below [10]. (See figure 3-4)

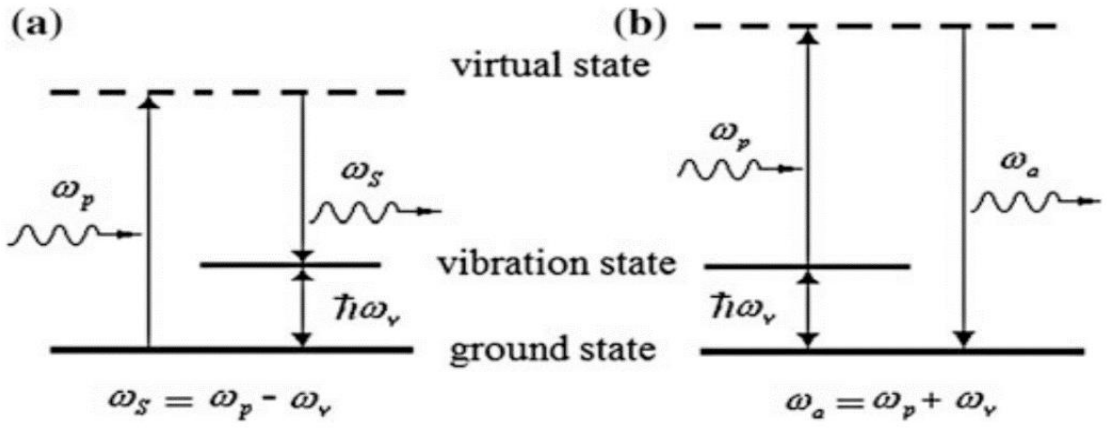

***Figure 3-2*- Illustration of energy-level diagram for explaining Raman scattering: (a) Stokes scattering ; (b) anti-Stokes scattering. Adapted from [10], page 153.**

Anti-Stokes Raman scattering is weaker in intensity compared to Stokes Raman scattering because it occurs in excited-state molecules. The formation process of Raman scattering is explained using the energy-level diagram shown in Figure 3-4 [17]. As a result, most Raman spectrometers are designed to utilize Stokes Raman scattering, which occurs in molecules in their ground state. During Raman scattering, the shift in the wavelength of the incident light corresponds to the unique vibrational energy of the molecule. The anti-Stokes line is several orders of magnitude weaker than the Stokes line.

Since each molecule possesses a distinct vibrational energy, the frequency shift is characteristic of the molecular composition or structure. Thus, Raman scattered light provides valuable insights into the chemical identity and structure of a substance [17].

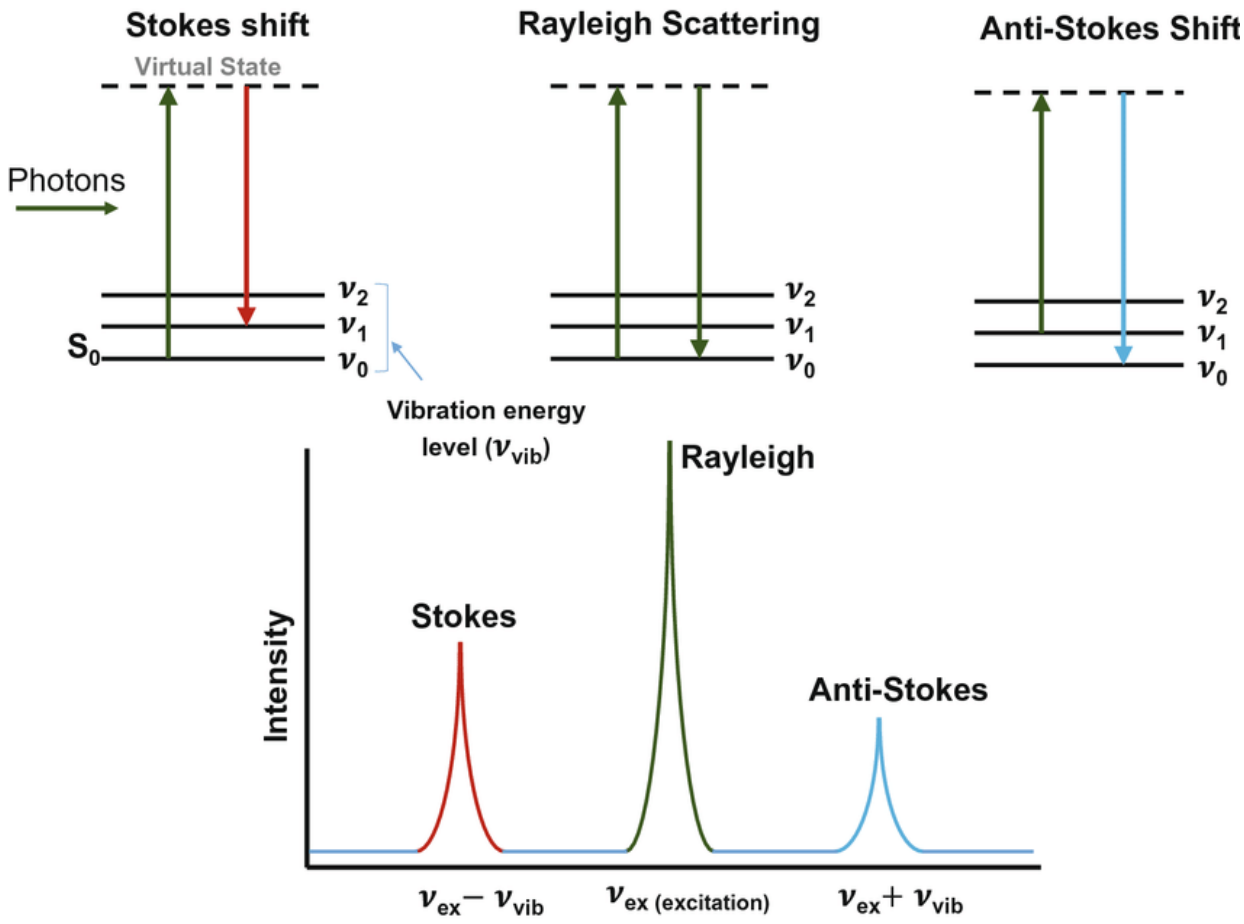

***Figure 3-3*- Energy-level diagrams for explaining Raman scattering, Stokes scattering, and anti-Stokes scattering. Adapted from [17].**

The process of Raman scattering is followed by a few steps. Firstly, a molecule in the ground state absorbs a pump light photon at energy level ν_0, transitioning to a virtual state. It then moves from this virtual state to the molecule vibrational (or rotational) state, simultaneously emitting a Stokes photon at energy level ν_1, as illustrated in Figure 3-4. Conversely, a molecule in the vibrational (or rotational) state absorbs a pump light photon at ν_1, jumping to another virtual state, then transitions from that virtual state to the ground state, emitting an anti-Stokes photon at energy level ν_1. Because in the thermal equilibrium case, the number of molecules in the ground state significantly exceeds those in the vibrational state, resulting in the number of photons at energy level ν_1 being much higher than at energy level of ν_2, resulting in higher intensity of Stokes than anti-Stokes [10].

The frequency and wave vectors of the incident photon are shown as "ω_p", "k_p", scattering photon shown by "ω_s","k_s" and the anti-Stokes photon is shown as "ω_a","k_a". They must satisfy the following energy and momentum conservation principles:

$$\omega_s = \omega_p - \omega_v \quad (3.12)$$

$$\omega_a = \omega_p + \omega_v \quad (3.13)$$

$$k_s = k_p - k_v \quad (3.14)$$

$$k_a = k_p + k_v \quad (3.15)$$

The stimulated Stokes scattering light and the stimulated anti-Stokes scattering light are generated simultaneously. In other words, the first-order anti-Stokes scattering light is produced through the interaction between the pump light and the first-order Stokes scattering light. These three components must satisfy the following wave-vector matching condition: [10].

$$\Delta k = 2k_p - k_s - k_a = 0 \quad (3.16)$$

3.3.1 Classical Theory of Stimulated Raman Scattering

We employ nonlinear coupled equations to examine the stimulated Raman scattering process. In an isotropic medium, a pump light field "$E_p(\omega_p)$" at frequency "(ω_p)" enters the medium, interacting with it to generate a Stokes scattering light "$E_s(\omega_s)$ at frequency "ω_s". Both fields propagate along the z-axis. Under the phase-matching condition, the nonlinear coupled equation for is given as follows:

$$\frac{dE_s(z)}{dz} = \frac{i\omega_s}{2\epsilon_0 c n_s} p^{(3)} z \quad (3.17)$$

And the nonlinear polarization is given as:

$$p_z^{(3)} = 6\varepsilon_0 X_R^{(3)}\left(\omega_{s;}\omega_p, -\omega_p, \omega_s\right)|E|_p^2 E_s(z) \quad (3.18)$$

Where $X_R^{(3)}\left(\omega_{s;}\omega_p, -\omega_p, \omega_s\right)$ is the susceptibility for Raman Stokes scattering light. It is possible to divide this into its real and imaginary components:

$$X_R^{(3)}(\omega_s) = X_R^{(3)}(\omega_s)' + iX_R^{(3)}(\omega_s)''(\omega_s) \quad (3.19)$$

The real part shows the refractive-index change (phase change), and the imaginary part shows the absorption coefficient change (energy change). Since we only study the energy exchange relation in the scattering process, we only need to discuss the imaginary part. Now, one can substitute relation (3.18) into (3.17) and use the imaginary part of the susceptibility $(+iX_R^{(3)}(\omega_s)'')$, one can obtain:

$$\frac{dE_s(z)}{dz} = -\frac{3\omega_p}{cn_s} X_R^{(3)}(\omega_s)''|E|_p^2 E_s(z) \quad (3.20)$$

To solve equation (3.20), we use the intensity relation $I_p = \frac{1}{2}\varepsilon_0 c n_p |E|_p^2$ and we replace $|E|_p^2$ by the light intensity I_p:

$$E_s(z) = E_{s0} \exp\left[\frac{-6\omega_s}{\varepsilon_0 c^2 n_p n_s} X_R^{(3)}(\omega_s) I_p z\right] = E_{s0} e^{\frac{1}{2} g I_p z} \quad (3.21)$$

Where g factor is:

$$g = \frac{12\omega_s}{\varepsilon_0 c^2 n_p n_s} X_R^{(3)}(\omega_s) \quad (3.22)$$

If $X_R^{(3)} < 0$, "g" shows a gain factor, which is a factor by which the input power is amplified. Below, we will see that (X_R'') is smaller than zero. As a result, the intensity of the Stokes-scattered light increases exponentially along the propagation direction (z-axis) [51].

3.4 Gas-filled hollow core fibers

In recent years, significant advancements in nonlinear and ultrafast optics have been achieved through the utilization of gas-filled HCF dielectric waveguides. Specifically, the phenomenon of SPM of laser pulses within these waveguides has enabled researchers [3, 34] to generate light pulses with durations as short as 4.5 femtoseconds. HCFs are instrumental in the generation of ultrashort pulses through multiple stimulated Raman scattering processes. Until recently, the prevailing approach in nonlinear-optical experiments with rare-gas jets centered on concentrated laser beams, aiming to achieve high power density. However, the efficiency of harmonic generation using this method is limited by the short interaction distances inherent in this beam configuration [52]. Miles et al. [15] proposed a method back in 1977 to enhance the length of nonlinear-optical interaction in a gas medium. They demonstrated the potential for a significant (by three orders of magnitude) increase in the efficiency of nonlinear-optical interaction within a hollow dielectric fiber. This was observed in a four-wave mixing process of coherent anti-Stokes Raman scattering [12].

To create a laser system that is both efficient and compact, with optimized pulse delivery and precise control over nonlinear applications in the high-energy regime, a comprehensive understanding of pulse propagation and nonlinear interactions within HCF operating in a multimode environment is essential [13]. In general, a waveguide—defined by its transverse optical properties as a function of position (x, y), can support multiple guided modes, typically represented by the mode field distribution $F(x, y)$. These modes form an orthonormal set, with each having a unique propagation constant "β". This concept is similar to the distinct energy levels or frequencies of eigenfunctions in a typical quantum mechanical system. A HCF is a basic type of waveguide, consists of a glass fiber surrounding an air-filled cylinder. Consequently, the boundary conditions resemble those of a hollow cylinder with a dielectric edge. Because of the symmetry problem, it is advantageous to use cylindrical coordinates "ρ", "ϕ", and "z". The radial origin is then located at the center of the inner circle, while the z-coordinate aligns with the axis of rotational symmetry. By applying the method of separation of variables, the modes of the system can be determined by solving a specific equation. (Equation 3.23) [13]

$$\frac{d^2F}{d\rho^2} + \frac{1}{\rho}\frac{dF}{d\rho} + \left(n^2k_0^2 - \beta^2 - \frac{m^2}{\rho^2}\right) = 0 \qquad (3.23)$$

Where "β" represents the propagation constant, "m" represents an integer, "k"$_0$ is the wavenumber at the central frequency, and "n" denotes the refractive index of the core. Light travelling through the HCF conforms to the weak guiding condition due to the insignificance of the longitudinal electric field components. Consequently, the fields within practical optical fibers primarily exhibit transverse characteristics, being described as Linearly Polarized modes (LP_{mn}). The first index (m) of the LP mode represents the intensity variation of light in the azimuthal plane (φ). For the fundamental mode, this index becomes 0, indicating that once the field direction is determined, the intensity remains constant at all angles "φ" for a given radial distance "ρ". The second index of the LP modes signifies the number of zero crossings in the light intensity pattern. This count is one less than the index itself. Thus, the LP_{01} mode, for example, exhibits no zero crossings in its intensity pattern, despite the intensity diminishing radially outward. In LP_{1n} modes, there is a single-cycle variation in light intensity in the azimuthal plane, resulting in m-1 zero crossings. Consequently, within the framework of the weakly guiding approximation, the LP_{01} mode emerges as the dominant mode of propagation [13]. The LP_{01} mode is the primary mode of propagation, and subsequently, all subsequent modes propagate similarly. Additionally, each mode exhibits intrinsic degeneracy attributed to the two orthogonal polarizations. Figure 3-5 illustrates the intensity patterns of various LP_{mn} modes, highlighting the several potential field patterns for each mode. When referring to the LP_{11} mode, we are describing four potential field patterns having polarization (two

orthogonal states) and intensity patterns ($LP_{11}a$ and $LP_{11}b$). Therefore, if an input pulse of arbitrary polarization excites the LP_{11} mode upon entering the fiber, the light propagating within the fiber is a combination of these four possible patterns (two orthogonal states and two intensity patterns) of the LP_{11} mode, all simultaneously present. Similar possibilities also apply to the LP_{01} mode, with the only distinction being the circularly symmetric nature of the intensity pattern. This symmetry means that any angular rotation of the pattern around the axis does not alter the intensity distribution, but simply changes the polarization orientation [13].

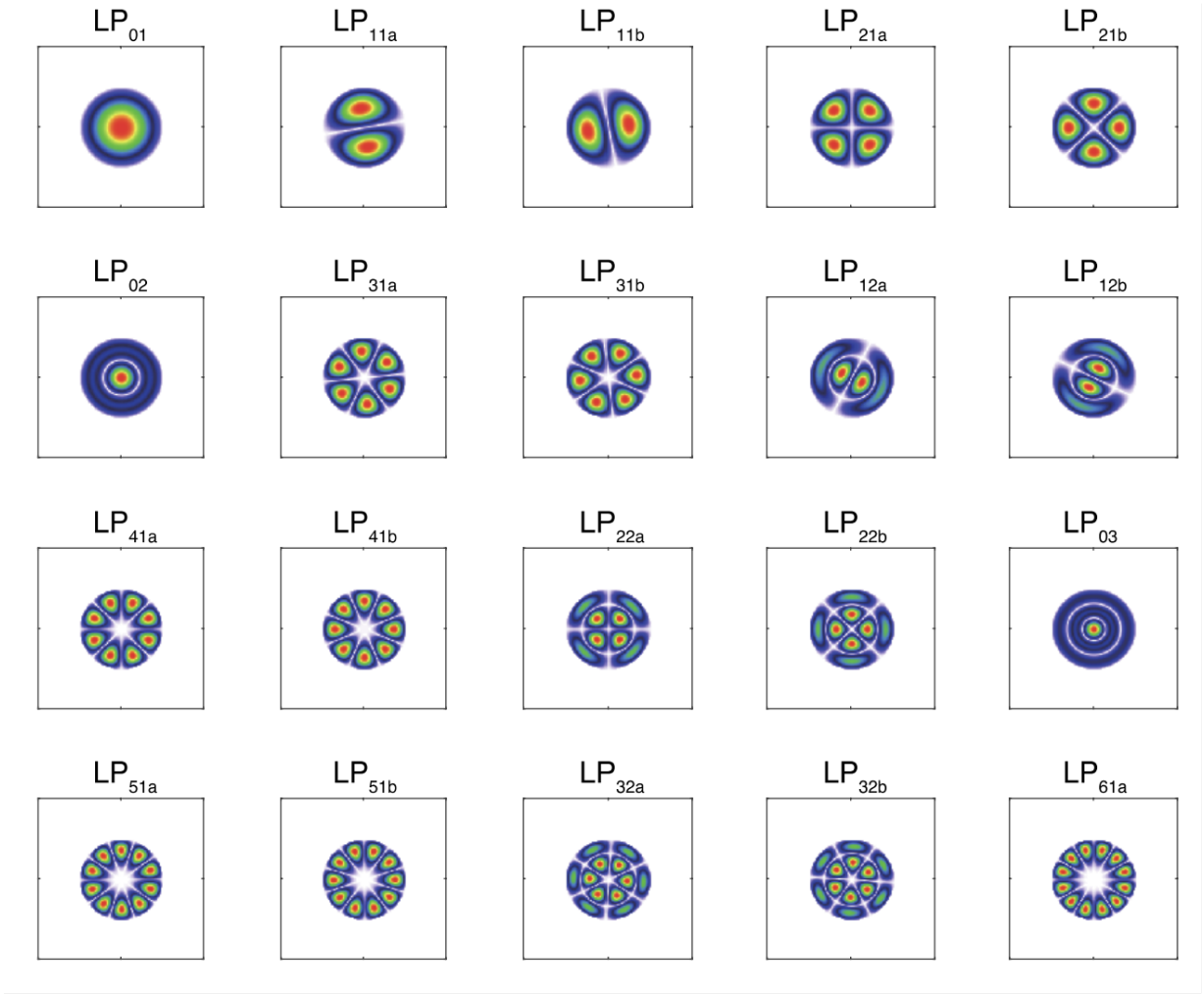

***Figure 3-4*- The intensity patterns of the selected modes. Adapted from [13], page 63.**

When a linearly polarized pump pulse is considered, there is the potential for nonlinear interactions between orthogonal polarization modes. This can result in phenomena such as birefringent phase matching and vector modulation instability. However, due to the description of modes as LP_{mn} modes,

when linearly polarized light is injected into the fiber, the nonlinear coupling to orthogonal polarization states is typically minimal. As a result, the majority of the pulse energy maintains its original polarization throughout the entire propagation. This characteristic enables a reduction in the number of modes to be accounted for in the model, offering computational advantages [13].

Modern advancements in laser physics have pushed the boundaries to the femtosecond regime, and a transition to attosecond pulses is anticipated in the near future. Light pulses with durations below 10 femtoseconds have already become commonplace in laser experiments, utilized for high-resolution spectroscopy, and generating radiation across a wide spectral range, including the water window, which is a biologically significant spectral region (2.3–4.4 nm) in soft X-rays. Additionally, light pulses shorter than 5 fs, generated through various methods in recent years, offer a unique capability to investigate a broad array of physical, chemical, and biological processes with exceptionally high temporal resolution, corresponding to just one or two optical cycles. Generation of pulses of orders sub-4 fs, achieved through the generation of multiple Stokes and anti-Stokes sidebands in a Raman-active gas, and the experimental demonstration of generating 250- attoseconds pulses (10^{-18}seconds) using phase-locking high-order optical harmonics was a remarkable recent achievement in the field of ultrafast science [12]. HCF filled with gas is a widely accepted compression technique. It has resulted in the generation of high-energy light pulses of the order of sub-5 fs. These ultra-short pulses have facilitated new applications in nonlinear optics, where the electric field of a light pulse undergoes significant intensity. Specifically, the employment of pulses spanning just a few optical cycles has been crucial for generating single attosecond pulses via HHG generation, as initially theorized by Christov et al. [53].

HCFs allow for phase matching between the pump and the signal produced in frequency-nondegenerate nonlinear-optical processes. By carefully adjusting the parameters of the HCF, including gas pressure and excitation of suitable waveguide modes, the phase mismatch caused by gas dispersion can be compensated for by the waveguide component of the phase mismatch [10, 54]. When these conditions are met, using longer HCFs can significantly boost the energy of the nonlinear signal. The parameters of short pulses of short-wavelength radiation generated through nonlinear-optical interactions in gas-filled HCFs can be managed via cross-phase modulation (XPM) [10, 54]. This concept was put into practice by Durfee et al. [38], who utilized XPM in parametric four-wave mixing in a gas-filled HCF to achieve efficient frequency up-conversion alongside pulse compression. By employing 35-fs pulses of Ti: Sapphire-laser radiation as a pump, Durfee et al. [12] successfully generated 8-fs pulses of 270-nm radiation after compensating for the chirp induced by XPM [12]. Employing HCFs enables the utilization of spatially

uniform SPM, surpassing the constraint on pulse energy imposed by the small core diameters of single-mode fibers. With its substantial and adaptable mode size, this method can accommodate significantly higher pulse energies compared to conventional single-mode optical fibers [55].

As the optical pulse travels through the HCF, changes in intensity across its width are minimal compared to changes in the electric field along its length, known as the paraxial approximation. Consequently, when the power is below a critical threshold (P < 0.3Pcr) for self-focusing, the evolution of individual modes is unaffected by each other [53]. Spectral broadening induced by SPM in gas-filled HCF can result in the generation of high-energy supercontinua, spanning more than two octaves. This offers the potential to generate pulses with a duration close to the transform-limited value of under 2 fs. In order to have around 98 % of power converted to the fundamental mode, it is essential to adjust the input beam size to approximately 64% of the core diameter of the HCF. This is because the fundamental mode exhibits the greatest degree of overlap with this Gaussian input beam [56].

3.5 Dispersion

Dispersion effects play a pivotal role in shaping the temporal and spectral characteristics of ultrashort pulses. Typically, the frequency-dependent dispersion of the refractive index in the gas inside the fiber causes distortion and broadening of light pulses. Moreover, dispersion effects limit the efficacy of nonlinear-optical interactions by inducing phase and GVD in light pulses [12]. Because the refractive index $n(\omega)$ varies with frequency, the wave number $k_n(\omega) = (\omega/c)\ n(\omega)$ within a dispersive medium, no longer follows a direct proportionality to frequency as it does in a vacuum, where $k(\omega) = \omega/c$. This nonlinear dependence of phase velocity on frequency, known as dispersion, is of great importance in ultrafast optics [26].

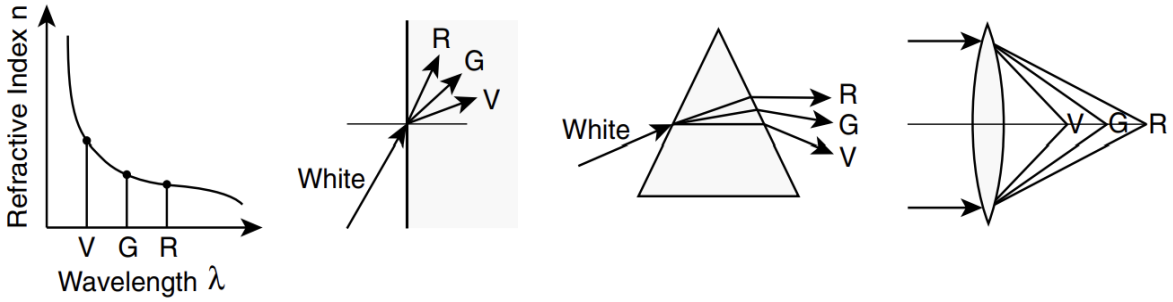

***Figure 3-5*- refraction resulting from dispersion of wave propagation. A dispersive medium with λ_R (red) > λ_G (green) > λ_V (violet). Adapted from [26], page 16.**

Another important example is the propagation of a light pulse through a dispersive medium (see Figure 3-7).

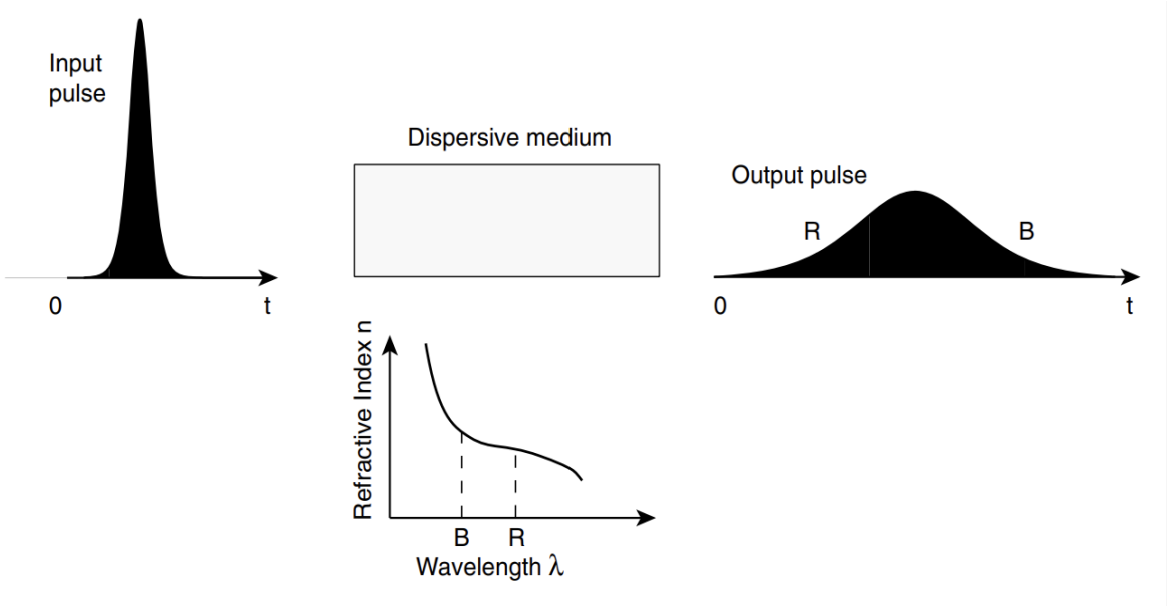

***Figure 3-6*- Dispersion on wave propagation as a result of pulse propagation in a medium. A normally dispersive medium, $\frac{d^2n}{d\omega^2} > 0$, or equivalently, $\frac{dv_g}{d\lambda} > 0$ which means the longer wavelength plane wave. Adapted from [26], page 17.**

Dispersion is commonly categorized into three types: normal or positive dispersion occurs when, $\frac{d^2n}{d\omega^2} > 0$, anomalous or negative dispersion arises when $\frac{d^2n}{d\omega^2} < 0$ and no dispersion is observed $\frac{d^2n}{d\omega^2} = 0$ [26].

3.6 Time-Bandwidth Product

In laser physics, the duration of a laser pulse "τ_p" is typically characterized by the full-width-at-half maximum (FWHM) of its time-dependent intensity profile. Similarly, the spectral width "$\Delta\nu_p$" of a laser pulse is usually determined by the FWHM of its spectral intensity. The shorter the pulse duration τ_p, indicating a smaller FWHM value, the broader the spectral width $\Delta\nu_p$. Using the Fourier transform as defined earlier, we can compute the time–bandwidth products $\Delta\nu_p \times \tau_p$ for various common pulse shapes. The specific values of the time–bandwidth product vary slightly depending on the pulse shape. The calculation of the time–bandwidth product for a Gaussian pulse is provided as an explicit example [26].

For a Gaussian pulse without chirp and with $I(t) = e^{-x^2}$, it can be calculated as $\Delta\nu_p \times \tau_p = 0.4413$ and for a Hyperbolic Secant (Soliton Pulse) $I(t) = sech^2 x$, one obtains $\Delta\nu_p \times \tau_p = 0.3148$.

3.7 Pulse Compression and Dispersion Compensation

The primary objective in the development of ultrafast laser oscillators is the shortest feasible laser pulse generation. First access to modern laser technologies helps researchers to obtain transforming outcomes. Spectra extending from 600 to 1200 nm have been generated from a Kerr-lens mode-locked Ti: Sapphire laser producing 5-fs pulses [57]. Even shorter pulses, down to 3 fs, are reachable by using external pulse compression methods. Although these ultrashort pulses have extremely broad spectral bandwidths, during propagation, they cause notable dispersive broadening [11]. Usually, two main approaches allow one to accomplish pulse compression. The first method is applying optical components linear characteristics. This method addresses pulse chirp by employing compensation methods. As compression instruments, for instance, Gires-Tournois interferometer mirrors and grating pairs have been used. This approach let Wang et al. produce 44-fs pulses with an energy of 531 nanojoules [58-60]. The other concerns are nonlinearity in optical fiber and dispersion adjustment. This approach compresses the light by changing its nonlinear properties and dispersion. Extensively building on the previous method, Verhoef et al. effectively produced fs pulses with an energy of 5-microjoules by using grating pairs as compressors and dispersion-compensating fibers as stretchers [61].

Generating pulses shorter than a picosecond requires consideration of GVD, a phenomenon that causes different frequency components to travel at different speeds, thus broadening pulses. Dispersion can be characterized by expressing the group delay, which corresponds to the first derivative of the phase shift φ(ω) of the optical system concerning frequency. This is expanded around the central frequency of the pulse spectrum, "ω_0" as follows: [62]

$$T_g(\omega) = \phi'(\omega_0) = \phi''(\omega_0)(\omega - \omega_0) + \frac{1}{2}\phi'''(\omega_0)(\omega - \omega_0)^2 \qquad (3.24)$$

Where $\phi'(\omega_0)$ represents the time that it takes for the pulse peak to travel through the dispersive medium. The higher-order terms in the expansion account for the frequency dependence of the group delay and are therefore responsible for dispersive effects. (ϕ'')also known as the group delay dispersion (GDD), refers to the lowest order group delay dispersion or second-order phase dispersion, and (ϕ'''), (ϕ'''') are the third-order and fourth-order dispersion, respectively [62].

Most laser and optical materials inherently exhibit positive group delay dispersion at 1um spectral region, meaning that the group delay increases with frequency. This results in a positive frequency sweep, or chirp, being introduced to pulses as they propagate through the medium. Ultrashort pulses, lasting only tens of femtoseconds, can undergo significant broadening even when traveling through just a few millimeters of transparent materials such as quartz or Sapphire. At higher intensities, this broadening intensifies due to SPM, which further broadens the pulse spectrum by introducing a positive temporal chirp. This positively chirped pulse can interact with a material with negative GDD to counteract this broadening. Additionally, negative GDD is used to compress pulses whose spectra have been broadened by SPM [62]. Pulses with a pulse duration of the order 7.5 fs have been generated by a Kerr-lens mode-locked Ti: Sapphire oscillator using chirped mirrors [63]. A powerful pulse compression technique based on spectral broadening in an HCF filled with noble gases has demonstrated the capability of handling high-energy pulses (sub-millijoule range) [55]. This technique provides the advantages of a guiding element with a large-diameter mode. Gas-filled HCF pulse compression experiments initially utilized 140 fs-input pulses. These trials resulted in the generation of FTL pulses of 18-fs and 10-fs pulses, achieving energies of up to 240 μJ [55].

4 PULSE CHARACTERIZATION FREQUENCY RESOLVED OPTICAL GATING

4.1 Frequency Resolved Optical Gating

Since the introduction of ultrashort pulse lasers, the technology for sensing ultrashort pulses has been developing alongside it. Early techniques could provide the pulse autocorrelation (AC) intensity, while later developments made it possible to indirectly estimate several phase distortions usually found in ultrashort pulses. However, these methods provided incomplete information, and iterative methods are employed to extract both the time-dependent intensity $I(t)$ and phase $\phi(t)$. However, uncertainties such as the temporal direction of the pulse remain, and determining characteristics like the sign of the chirp often requires an additional measurement after propagation through a known dispersive medium. Other characterization techniques require a streak camera, which compromises temporal resolution, or a reference that increases the complication of execution [15].

The FROG method, which was introduced first by Rick Trebino in 1993, can make use of any almost immediate nonlinear optical response [80]. It is used to fully characterize ultrashort laser pulses, measuring both intensity and phase as a function of time or frequency based on nonlinear optical interactions.

4.2 SHG-FROG: Measurement, Theory, and Data Processing

A pulse is described mathematically by its electric field:

$$E(t) = Re\{A(t)e^{i(\omega_0 t - \phi(t)}\} \quad (4.1)$$

Where "$A(t)$" is the time-dependent intensity amplitude, "ω_0" is the carrier frequency and "$\phi(t)$" is the phase as a function of time. The goal of FROG is to measure both "$A(t)$ " and "$\phi(t)$" completely [14].

FROG works by measuring a two-dimensional trace in the time-frequency domain, known as the FROG spectrogram (relation 4.1). The optical implementation of FROG involves generating a gating effect through the nonlinear interaction between the pulse and a time-delayed version of itself. However, instead of a direct measurement, the data is collected using a spectrometer, where critical information is recorded in terms of the spectrum versus delay [64].

The FROG method involves dividing the pulse into two identical copies and directing them through a nonlinear optical element with a controllable time delay introduced between the copies. The nonlinear signal is then spectrally analyzed based on this time difference. In SHG-FROG, the nonlinear signal is a

noncollinear AC signal generated typically from a SHG crystal, such as a barium-borate (BBO) crystal, doubling the frequency. The shape of the envelope of the SHG-FROG signal field is defined as:

$$E_{sig}(t,\tau) = E(t)E(t-\tau) \qquad (4.2)$$

Where "$E(t)$" is the complex envelope of the pulse to be measured and "τ" is the delay between the two beams. The resulting signal is incident on a spectrometer, which then records a FROG trace. The intensity of the signal can additionally be recorded on a photodiode.

$$I_{FROG}(\omega,t) = \left|\int_{-\infty}^{\infty} dt\, E_{sig}(t,\tau)\exp(i\omega t)\right|^2 = \left|E_{sig}(t,\tau)\right|^2 \qquad (4.3)$$

Where "I_{FROG}" is the measured intensity of the spectrogram, and "E_{sig}" is the signal field, which varies depending on the type of FROG. Figure 4-1 represents our FROG setup in the ALLS lab and FROG schematic. We have used a D-shape mirror in our setup to generate a replica of the pulse instead of a beam splitter.

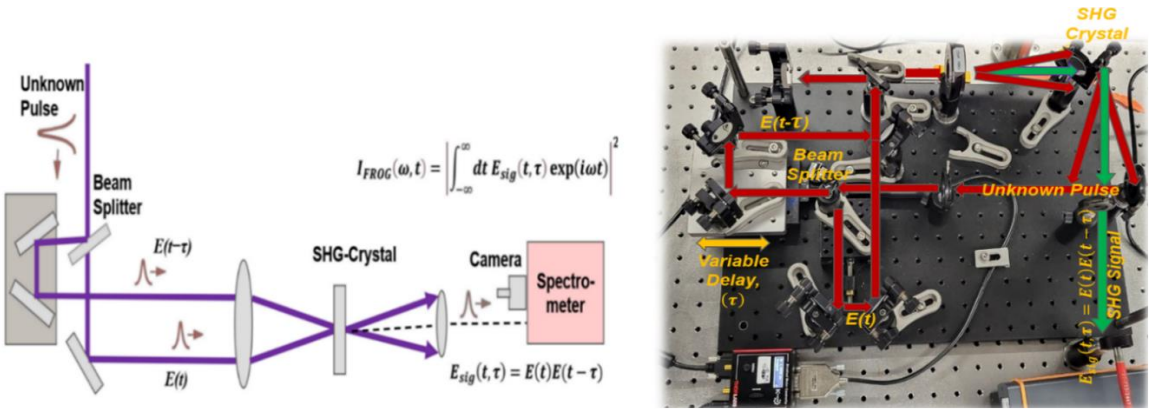

***Figure 4-1*- The process starts with the pulse in the red arrow. After passing through an iris, it goes through the D-shape mirror. Pulse1, $shown\ as\ E(t)$, is reflecting from two 45-degree mirrors, and then it reaches the BBO crystal, while pulse2, shown as $E(t-\tau)$, is first passing through the delay stage. Finally, the two pulses overlap in the BBO crystal, and the superposition of the two pulses creates the third pulse (SGG signal) shown in the green arrow. At the end of the setup, there is a spectrometer to record the spectrogram. Adapted from [65].**

A FROG measurement records spectra for different arrangements of arrival time differences of two pulses, resulting in creating a FROG trace known as a spectrogram representing intensity as a function of time delay and optical frequency or wavelength [66]. In order to obtain the pulse shape from the FROG trace, an iterative phase retrieval algorithm using a computer program is used. The retrieval algorithm continues until the recorded data are almost similar. Afterwards, the FROG retrieval algorithm shows the pulse shape. In this technique, a shorter gate pulse plays a role as a sample from a longer pulse, utilizing nonlinear

interaction mixing (gating) in a nonlinear crystal medium. In this case, since a gate pulse shorter than the original pulse does not exist, FROG uses a replica of itself to do the process [66].

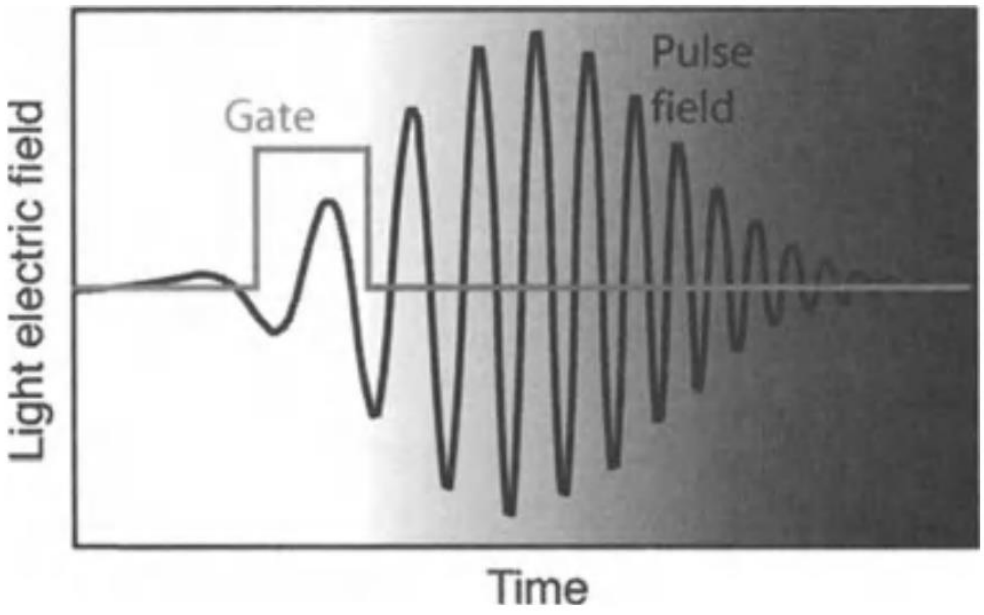

***Figure 4-2- Depiction of a spectrogram using graphics. A gate function gates out a piece of the waveform (in this case, a linearly chirped Gaussian pulse), and the spectrum of that piece is computed or measured. Therefore, the gate is scanned through the waveform, and the process is repeated for all values of the gate position (i.e., delay)*. Adapted from [67], page 102.**

The FROG trace represents a positive real-valued function of two parameters: the frequency and the time delay between the two pulses. The measured FROG trace is provided as an input to a computational algorithm, which calculates the complex electric field, both phase and intensity, of the pulse that generated the FROG trace. It should be noticed that the signal field described by relation 4.2 remains unchanged, apart from a minor temporal shift, when the delay time experiences a change in sign. Consequently, the SHG-FROG trace exhibits symmetry around zero delay time: $I_{FROG}(\omega, t) = I_{FROG}(\omega, -t)$. This results in an uncertainty in the recovered electric field regarding the direction of time, i.e., the field $E(t)$ produces the same FROG trace as $E^*(-t)$ (The presence of the complex conjugate arises because we are considering only positive frequency components of the field.) This temporal uncertainty is the primary drawback of SHG-FROG compared to a $\chi(3)$ FROG method. This ambiguity in the retrieved field also results in unintuitive traces that can make pulse-retrieval using the algorithm difficult.

To illustrate this, consider a pulse with a Gaussian intensity profile and a linear chirp:

$$E(t) = \exp(-at^2 + ibt^2) \qquad (4.4)$$

The normalized SHG-FROG trace of this field is:

$$I_{FROG}(\omega, \tau) = \exp\left[\frac{-4\left(a^3+ab^2\right)\tau^2 - a\omega^2}{4(a^2+b^2)}\right] \qquad (4.5)$$

Where "a" and "b" are real parameters characterizing the pulse; "a" determines pulse duration (larger "a"results in shorter pulse duration) and "b" shows the chirp parameter. The SHG-FROG trace of a linearly chirped pulse forms an upright elliptical shape, regardless of the sign of the chirp parameter (b). The SHG-FROG trace remains the same for a pulse exhibiting either positive or negative linear chirp. This stands in contrast to PG-FROG traces, where pulses with positive or negative linear chirp result in ellipses tilted to have either a positive or negative slope, respectively, facilitating the easy differentiation between positive and negative chirp. Overall, SHG-FROG cannot distinguish between a pulse and its time-reversed counterpart [14].

This technique (relation 4.5) enables the reconstruction of the spectral phase using an appropriate inversion algorithm. FROG represents a two-dimensional phase retrieval challenge with a unique solution—retrieving the FROG trace is essentially an inverse problem, where the goal is to align the available solution with the correct formulation [64] .We have recorded FROG traces of fundamental pulse (780nm) under vacuum in the Advanced Laser Light Source (ALLS) lab using a Ti: Sapphire laser with a central wavelength of 780-800 nm, repetition rate of 100Hz, and initial time duration of 60 picoseconds. This process took a few minutes for each record. Experimental and reconstructed FROG trace of the fundamental pulse measured in the ALLS lab, generated by a 780 nm Ti: Sapphire fs laser, is shown in Figure 4-3.

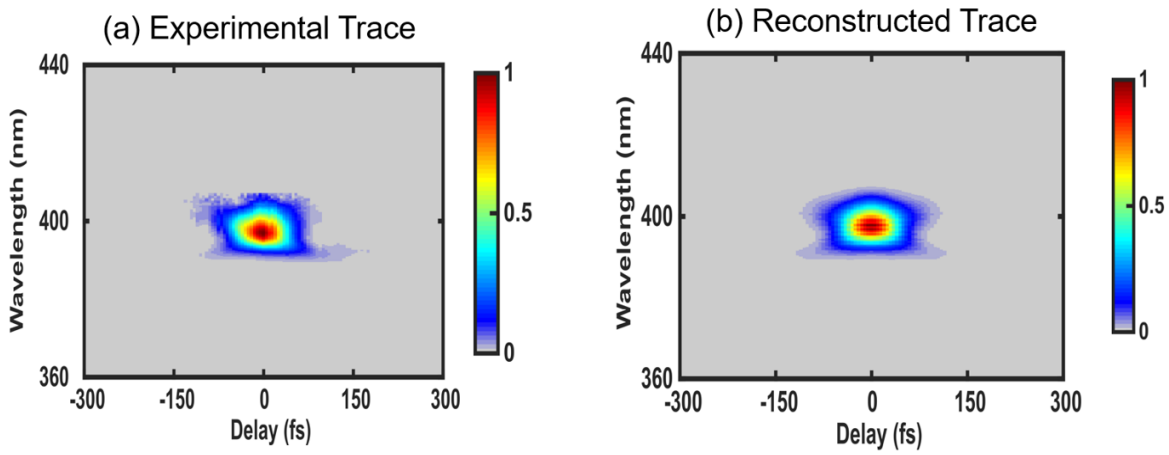

***Figure 4-3*-(a) experimental and (b) reconstructed traces, the color bar shows the intensity scale.**

4.3 Types of FROG

Different FROG methods exist based on the nonlinear optical interaction used to generate the signal. Each type has unique advantages and disadvantages [16].

1. Second-Harmonic Generation FROG (SHG-FROG): SHG-FROG is the most commonly used FROG method, involving second-harmonic generation in a nonlinear crystal. It measures the AC of the pulse with itself. It provides high sensitivity but has a time-direction ambiguity, meaning it cannot determine whether a pulse is forward or time-reversed. This is of significant importance in pulse compression and dispersion compensation. If this ambiguity is not resolved while removing chirp from the pulses to be compressed to their limited-transform duration, the wrong dispersion may lead to generating a longer pulse. This method is suitable for measuring weak pulses from Ti: Sapphire oscillators [16].

2. Third-Harmonic Generation FROG (THG-FROG): THG-FROG extends SHG FROG by using a third-order nonlinearity to generate third-harmonic signals. It is more sensitive than SHG but has some phase ambiguities for multiple pulses, and this method is an effective way for measuring ultrashort pulses. (See Table 4.1 for more details) [16].

3. Polarization-Gate FROG (PG-FROG): PG-FROG relies on the Kerr effect, where the pulse intensity modulates a polarization gate in a third-order nonlinear medium. There are no known ambiguities, and it provides intuitive traces. However, it requires high-quality polarizers, making it unsuitable for deep UV pulses [16].

4. Self-Diffraction FROG (SD-FROG): SD-FROG uses self-induced gratings in a Kerr medium to generate a diffraction signal. SD-FROG is similar to PG FROG but more sensitive to even-order phase distortions. It avoids using polarizers but requires a thin medium, for example, fused silica ($> 200\ \mu m$) to minimize phase mismatch [16].

5. Transient-Grating FROG (TG-FROG): TG-FROG uses a transient grating formed by two beams to diffract a third beam, producing the signal. It is sensitive and background-free. Moreover, it is the best for measuring amplified ultrashort pulses, but it requires three beams, and the alignment is also complicated [16].

6. TADPOLE (Spectral Interferometry): TADPOLE (Temporal Analysis by Dispersing a Pair of Light E-fields) is not a FROG method but a spectral interferometry technique that uses a reference pulse for high sensitivity. This method is an appropriate choice for measuring extremely weak pulses (as low as one photon per pulse). It uses a reference pulse measured via FROG to retrieve an unknown pulse. However, it is not a true FROG method but is often used in conjunction with FROG.

Figure 4-4 represents a schematic of different FROG types of geometry. Table 4.1 summarizes signal field expression and sensitivity for various types of FROG. [16]

Second-order and third-order nonlinearity are ideal approaches. There are some advantages to the third-order nonlinearity approach. The $\chi^{(3)}$FROG trace is useful as a real-time pulse parameter monitor since, for most pulses of interest, it essentially shows the instantaneous frequency over time. By contrast, FROG traces produced with SHG-FROG are less obvious and not as appropriate for real-time pulse monitoring. Additionally, in contrast to third-order techniques, second-order procedures generate a time-reversal ambiguity, which can be problematic. However, in situations when pulse intensities are restricted—usually below about 1 MW—a second-order technique is beneficial since its signal is stronger than that of third-order techniques [14].

Since the efficient frequency doubling is strongly dependent on phase matching, it is important to highlight that the thickness of the crystal used in SHG-FROG plays a crucial role—thinner crystals allow the measurement of pulses with broader bandwidths. In thick crystal fundamental and second harmonic generated signal experience different group velocities, leading to a reduction in pulse measurement accuracy, the thinner crystal minimizes phase matching restriction, which allows a wider range of frequencies to contribute to SHG. In our experiment, a 25 µm-thick BBO crystal was used. It is worth noting that the temporal ambiguity only impacts phase distortions that exhibit even functions of time. For

instance, a linear chirp, characterized by a quadratic temporal phase dependence, encounters an ambiguous sign in SHG-FROG. However, phenomena such as frequency shifts (which entail linear phase changes over time) or temporal cubic phase distortions (displaying cubic phase alterations over time) do not entail an ambiguous sign. The reason is that SHG is a nonlinear process in which a photon with frequency "2ω" is generated using two photons at frequency "ω" by squaring the electric field and the phase information will transform as below:

$$E_{SHG}(t) \sim E(t)^2; \quad ; \quad \Phi_{SHG}(t) = 2\Phi(\mathrm{t}) \qquad (4.6)$$

It means that even-order phase terms, such as quadratic, do not change, though even-order phase terms reach their original sign and direction. Often, prior knowledge about the pulse is known that can assist in resolving this ambiguity. For instance, pulses typically acquire a positive linear chirp (unless operating in the negative GVD regime) due to propagation through standard optics. Therefore, we can sometimes assume that the pulse has an overall positive chirp and establish a time direction. Additionally, in the case of high-intensity pulses, $\left(10^{12}\ {}^{TW}/_{cm^2}\right)$ SPM may play a role. If the sign of the nonlinear refractive index "n_2" is known, the time direction can be determined by specifying the appropriate sign of the phase [14]. It is important to note that while the SHG-FROG trace exhibits symmetry with respect to "t", this limitation does not extend to the pulse obtained through the algorithm. Since the measurement in SHG-FROG is based on the intensity (electric field squared) rather than the electric field, the phase information that leads to distinguishing the pulse from its time-reversed is lost. Therefore, the SHG-FROG trace for $E(t)$ is the same as its time-reversed, $E(t-\tau)$. It also creates a signal frequency that is doubled the initial frequency using the same temporal profile, leading to keeping the temporal symmetry. If we utilize a temporally asymmetric pulse to generate a SHG-FROG trace, the pulse-retrieval algorithm will produce that asymmetric pulse (or its time-reversed replica).

After generating the FROG trace experimentally in the laboratory, the next step involves applying a numerical algorithm to the data to extract the complete complex envelope. This algorithm is rooted in iterative Fourier-transform algorithms commonly employed in phase-retrieval techniques. The family of FROG algorithms proves to be more resilient compared to conventional phase-retrieval algorithms, partly due to the constraint outlined by Equation 4.3, which is not present in other techniques such as image-recovery. The original basic FROG algorithm that was initially developed for PG-FROG is not as effective for SHG-FROG as it is for PG-FROG. A slightly adjusted version of this algorithm, which includes the application of a spectral constraint, has been proposed specifically for SHG-FROG, referred to as the modified basic

algorithm. None of these algorithms converges effectively for the types of pulses commonly observed. Therefore, it has become necessary to introduce a more mathematically robust algorithmic technique known as generalized projections [14].

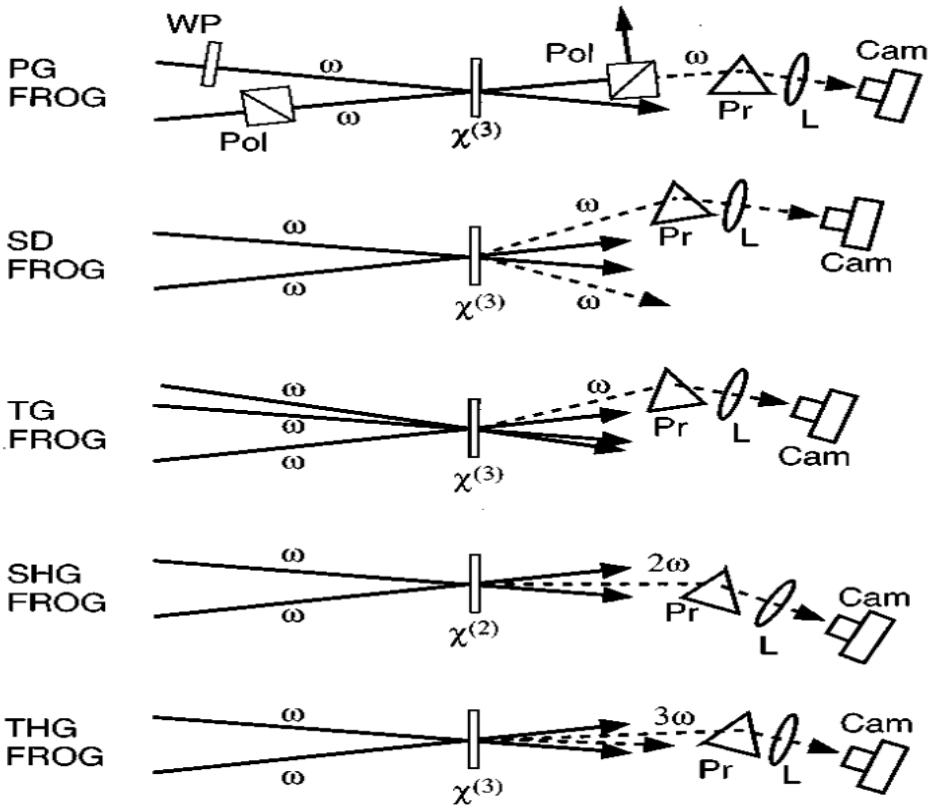

***Figure 4-4*-Diagrams illustrate five distinct beam geometries used for FROG measurements of ultrashort laser pulses: polarization gate (PG), self-diffraction (SD), second-harmonic generation (SHG), third-harmonic generation (THG), and transient grating (TG) FROG. Solid lines represent input pulses, while dashed lines denote signal pulses. The nonlinear medium properties are indicated, along with key optical components: Pol (polarizer), WP (wave plate), Pr (prism), L (lens), and Cam (camera). Each setup includes a prism-lens combination as a generic spectrometer, which may also use a grating or other dispersive elements instead of the prism. Delay lines and additional lenses, common to all configurations, are not shown. The labeled frequencies (v, 2v, 3v) indicate whether the signal pulse retains the same carrier frequency as the input pulse or undergoes a frequency shift, as seen in SHG and THG. Adapted from [16], page 3282.**

Table 4-1 Summary Table of FROG Types. Adapted from [16].

Type	Signal Field $E_{sig}(t,\tau)$	Sensitivity (Single Shot)	Sensitivity (multi-shot)
SHG-FROG	$E(t)E(t-\tau)$	~0.01 μJ	~0.001 nJ
THG-FROG	$E(t)^2E(t-\tau)$	~0.03 μJ	~3 nJ
PG-FROG	$E(t)E(t-\tau)^2$	~1 μJ	~100 nJ
SD-FROG	$E(t)^2E^*(t-\tau)$	~10 μJ	~1000 nJ
TG-FROG	$E(t)E^*(t-\tau)$	~0.1 μJ	~10 nJ

Figure 4-5 represents the FROG traces for different geometries of ultrashort light pulses.

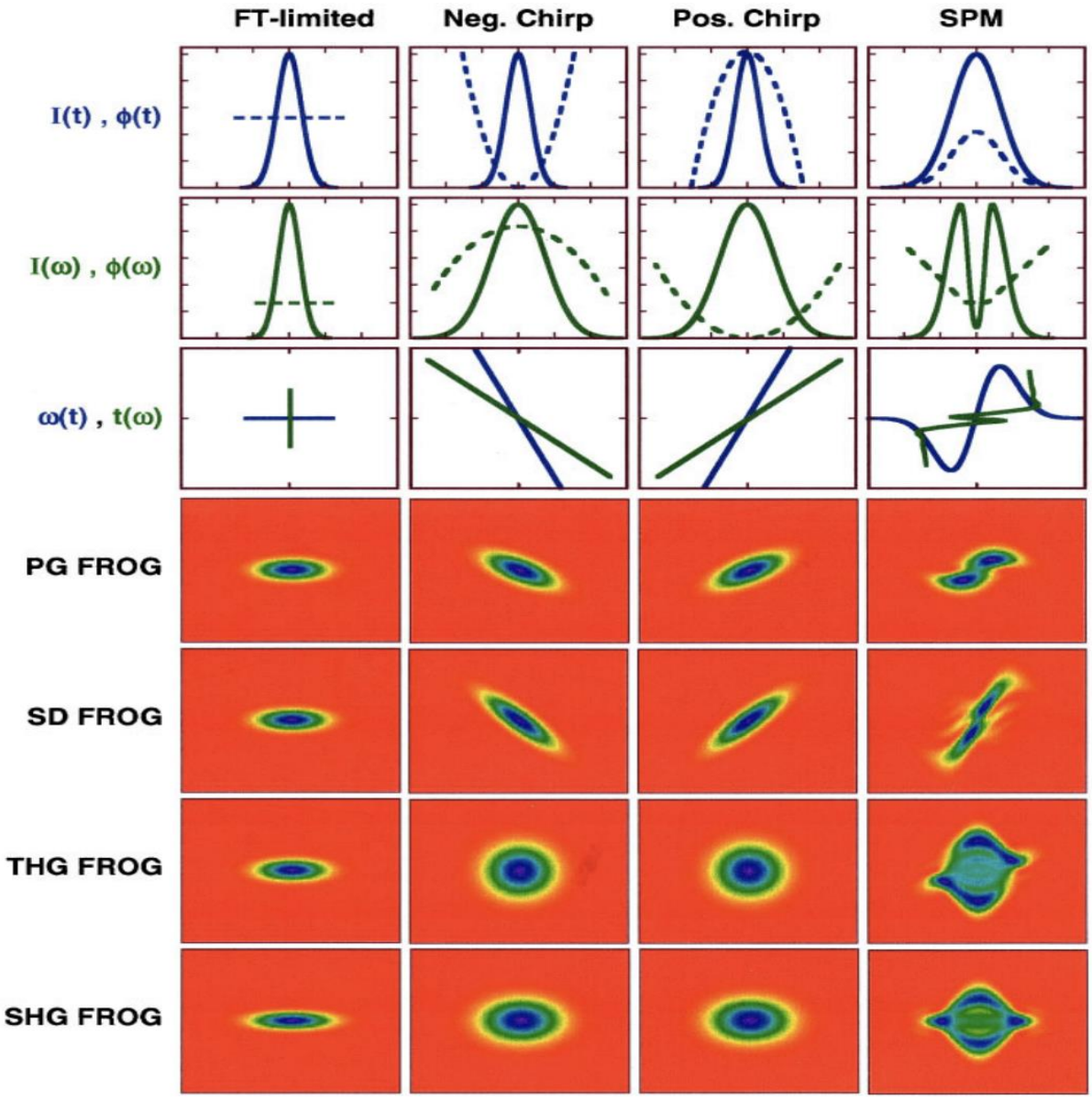

***Figure 4-5*- Illustration of the FROG traces for different geometries of typical ultrashort light pulses. The first row shows pulse intensity I(t) (solid line) and phase w(t) (dashed line) over time, while the second row presents the spectrum $\tilde{I}(v - v_0)$ (solid) and spectral phase $\tilde{\omega}(v - v_0)$ (dashed). Phase increments are marked in steps of π radians. The third row displays instantaneous frequency v(t) (blue) and $\tilde{t}(v)$group delay (green), with $\tilde{t}(v)$ plots rotated due to differing time and frequency axes. Arrows indicate infinities. The last four rows show false-color FROG traces (purple for high intensity, red for low) for PG, SD, SHG, and THG geometries. TG FROG traces match PG or SD, depending on pulse delay. PG and SD traces reflect either frequency vs. time or group delay vs. frequency. THG traces are more symmetrical and less intuitive, while SHG traces, being perfectly symmetrical, introduce a time-direction ambiguity. Adapted from [16], page 3280.**

As previously mentioned in section 4.3, FROG relies on the formation of a nonlinear gating mechanism, with the most widely used variant known as SHG-FROG. SHG-FROG is highly reliable and sensitive for pulse

characterization but requires phase matching for SHG, which depends on input wavelength and pulse duration [16].

4.4 Generalized Projection

In addition to the enhanced algorithm discussed in the previous section, there is a mathematical principle known as generalized projections. Projections provide a straightforward means to conceptualize how these iterative algorithms operate, facilitating a robust implementation that significantly enhances the effectiveness of the FROG algorithm. Here, we will explain the idea of generalized projections.

In the FROG algorithm, our objective is to identify a signal field, $E_{sig}(t,\tau)$, that meets two criteria. Firstly, its FROG trace, as determined by Eq.(4.7) below, must align with that of the experimental data (constraint 1). Secondly, it must represent a field achievable through a physically realizable electric field, as defined by relation (4.8) (constraint 2). We can envision a function space comprising complex two-dimensional functions, with each point representing a potential $E_{sig}(t,\tau)$, Consequently, the values of $E_{sig}(t,\tau)$ satisfying the previous constraints from two distinct sets, each corresponding to one constraint. The intersection of these sets denotes the correct solution, illustrated in Figure 4-6. Once this accurate value of $E_{sig}(t,\tau)$, is ascertained, determining the appropriate form of $E(t)$ becomes straightforward. The FROG algorithm, as illustrated in Figure 4-6, initiates with a tentative solution for the field $E(t)$. Subsequently, a signal field is derived from this initial field using (4.2), followed by a Fourier transformation into the (ω, τ) domain. The squared magnitude of this frequency-domain signal field, denoted as $E_{sig}(\omega,\tau)$, corresponds to the FROG trace of the initial field $E(t)$. The first projection is then applied, wherein the magnitude of this frequency-domain signal field is constrained to match the magnitude of the experimentally obtained FROG trace. This is achieved straightforwardly by replacing the magnitude of the frequency-domain signal field with the square root of the experimental FROG trace, while retaining the original phase.

$$E'_{sig}(\omega,\tau) = \frac{E_{sig}(\omega,\tau)}{\left|E'_{sig}(\omega,\tau)\right|}\left[I_{FROG}(\omega,\tau)\right]^{1/2} \quad (4.7)$$

Relation 4.7 forms the projection leading to relation 4.8. An inverse-Fourier transform returns the signal to the time domain, resulting in $E'_{sig}(t,\tau)$. The metric utilized to gauge this proximity is defined by: [8]

$$z = \sum_{t,\tau=1}^{N}\left|E'_{sig}(t,\tau)\right|E(t)E(t-\tau)^2 \quad (4.8)$$

The term on the right-hand side within the squared modulus, $E(t)E(t-\tau)$, generates a new signal field guaranteed to adhere to constraint set 2. To determine the new signal field closest to $E'_{sig}(t,\tau)$, we minimize Z concerning $E(t)$. This minimization yields the field corresponding to the projection of $E'_{sig}(t,\tau)$ onto the set of fields satisfying Eq. (4.8). This projection provides us with the estimation of $E(t)$ for the subsequent cycle of the algorithm. In practice, a global minimization of the error is not typically required. Instead, a single one-dimensional minimization along the direction of the analytically computed gradient of Z appears to suffice and is computationally more efficient. It involves treating the error as a single-valued function of $2N$ variables, representing the real and imaginary parts of $E(t)$ at each of "N" sampling points of the field array [14].

FROG algorithm autonomously monitors its progress for stagnation and employs alternative methods as needed to ensure maximal convergence. The combination of the generalized projection approach with the other strategies of the composite algorithm yields a remarkably potent method [14].

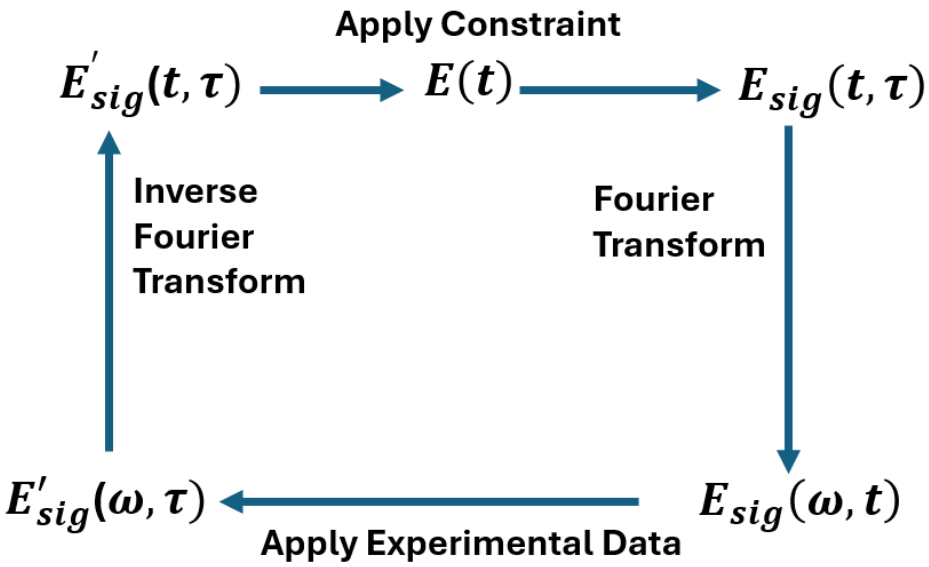

***Figure 4-6*- Schematic of the FROG pulse-retrieval algorithm. Adapted from [14].**

The development of FROG techniques has marked a significant advancement in ultrashort pulse characterization. Unlike earlier methods that provided only partial information, FROG enables the complete retrieval of both the intensity and phase of an optical pulse, overcoming fundamental ambiguities such as time-direction uncertainty. SHG-FROG remains one of the most widely used methods

due to its sensitivity and reliability. Advanced computational techniques such as generalized projections have been introduced as well. These iterative algorithms have enhanced the accuracy and robustness of pulse retrieval, making FROG a powerful tool for applications ranging from high-resolution spectroscopy to ultrafast optical communications. Future developments may further refine these techniques, incorporating machine learning and adaptive algorithms to enhance retrieval speed and accuracy, paving the way for real-time ultrashort pulse analysis [16].

5 VIBRATIONAL SRS IN CH_4

5.1 SRS as Frequency Shifting in HCF

The ability of SRS in gas-filled HCFs to produce notable frequency shifts—which are important in many optical uses—has been well investigated. One interesting example is the work of Benabid et al., [18] on SRS in hollow-core photonic crystal fibers filled with hydrogen. Their experiment was conducted using a 1-meter-long hollow-core photonic crystal fiber with a 15-micrometer-diameter core with hydrogen gas under pressure. By using a pulsed laser source with a duration of 6 nanoseconds at a wavelength of 532 nanometers, they observed that the threshold for the generation of Stokes light is at pulse energies as low as 800 ± 200 nanojoules. The threshold for coherent anti-Stokes generation was 3.4 ± 0.7 microjoules. At a pulse energy of only 4.5 microjoules, the pump-to-Stokes conversion efficiency attained 30 ± 3%. These results indicate that gas-based nonlinear optics could be achieved in parameter regimes with high intensity and long interaction lengths, which were previously considered unattainable [18]. Chen et al. [68] investigated the soliton self-frequency shift phenomenon in hydrogen-filled HCFs in another work. They found that solitons produced by inserting ultrashort 40-femtosecond pulses into the hydrogen-filled fiber underwent a continuous redshift owing to SRS. The efficiency of hydrogen-filled HCFs in applications involving soliton dynamics and SRS-induced frequency shifts is demonstrated by the effective frequency shifting achieved employing this phenomenon [68]. These investigations provide an understanding of the mechanisms and uses of stimulated Raman scattering in enabling frequency shifts within HCFs filled with various gases, therefore guiding the design of such systems. In this work, we investigate the use of gas-filled HCF as a platform for efficient SRS-based frequency conversion and pulse compression, enabling the generation of high-energy, ultrashort pulses using CH_4. The experimental setup and the obtained data from this experiment are shown in the following sections.

5.2 Experimental Setup

The experiments were conducted in the ALLS lab using a 780 nm Ti: Sapphire laser with an initial pulse duration of 60 fs (40 fs for FTL pulse duration). A diffraction grating method was used to broaden the pulse up to 3-ps. It was then coupled into a 1-meter HCF of 500-micron core diameter filled with CH_4 to start SRS. Figure 5-1 shows our experimental setup.

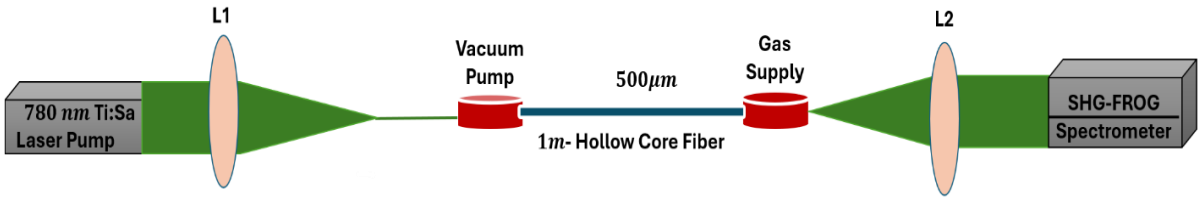

Figure 5-1: **Experimental Setup. L1 represents the focusing lens for coupling into HCF, and L2 shows the collimating lens after HCF.**

5.3 New Spectral Components generated due to Vibrational SRS

We utilized a Ti: Sapphire laser source with a central wavelength of 780 nm and an initial pulse duration of 3-ps (3000 fs, after stretching using grating position). Under vacuum conditions (pressure = 0.1 mbar), the pulse duration was measured as 1.1 ps. After injecting CH_4 gas into the fiber at 1000 mbar, no SRS peaks were observed, and the measured output energy remained at $400\ \mu$J. At 2000 mbar of CH_4, fundamental mode, first Stokes as well as anti-Stokes components were observed. At 2000 mbar pressure, using a long-pass filter (LP1000), the first Stokes peak was observed, and the pulse autocorrelation measured indicated a duration of 700–800 fs. After injecting 3000 mbar of CH_4 gas, we observed the fundamental mode (LP_{01}), first and second Stokes mode (LP_{02} and LP_{12}). Input and output energies $E_{in} = 400\ \mu$J and $E_{out} = 280\ \mu J$ along with a transmission of 70% was measured. Using a long pass spectral filter (LP1000), an output energy of $E_{out} = 103.7\ \mu$J an RMS fluctuation of 10% was measured. By introducing the short pass filter (SP785) and SP1319, we were able to observe anti-Stokes and both first and second Stokes components. Table 5-2 summarizes the energies and RMS of each Stokes.

Table 5-1: **Energy and RMS of first and second Stokes**

Energy of the first Stokes and RMS	Energy of the second Stokes and RMS	Energy of anti-Stokes and RMS
E=110.3 μJ, RMS=9.7	E=37.33μJ, RMS=35.33	E=38.44 μJ, RMS=33.8

The anticipated wavelengths of Stokes and anti-Stokes components from vibrational SRS in CH_4 can be calculated using the vibrational Raman shift and the input (pump) wavelength. The Raman-shifted wavelengths are derived from energy conservation as follows:

$$\frac{1}{\lambda_{Stokes}} = \frac{1}{\lambda_{Pump}} - n\,\Delta\upsilon_{Raman} \quad (5.1)$$

$$\frac{1}{\lambda_{Anti-Stokes}} = \frac{1}{\lambda_{Pump}} - \Delta\upsilon_{Raman} \quad (5.2)$$

Where"n" represents the Stokes order and "Δv_{Raman}" is referred to as vibrational Raman shifts. The vibrational Raman shifts for CH_4 is approximately $(2917\ cm^{-1})$ [1], and the pump laser is at $780\ nm$. Then $(\lambda_{First\ Stokes} \approx 1030\ nm)$, $(\lambda_{second\ Stokes} \approx 1470\ nm$ and $(\lambda_{Anti-Stokes} \approx 649\ nm)$ are obtained using relations (5.1) and (5.2).

5.3.1 Pulse characterization of First Stokes

The reconstructed and original traces shown below illustrate the pulse evolution under various experimental conditions. The original traces represent experimentally measured FROG signals, while the reconstructed traces are obtained through numerical retrieval algorithms, as discussed in Chapter 4, confirming the accuracy of the pulse characterization. Figure 5-2 represents the first Stokes pulse results

[1] https://webbook.nist.gov/cgi/cbook.cgi?ID=C74828&Mask=800

at 2000 mbar of CH_4, initial pulse duration of 3 ps and input energy of 2.5mJ. 2000 mbar of CH_4, initial pulse duration of 3 ps and input energy of 2.5mJ. Spectral filters LP1000 and SP1326 were also applied.

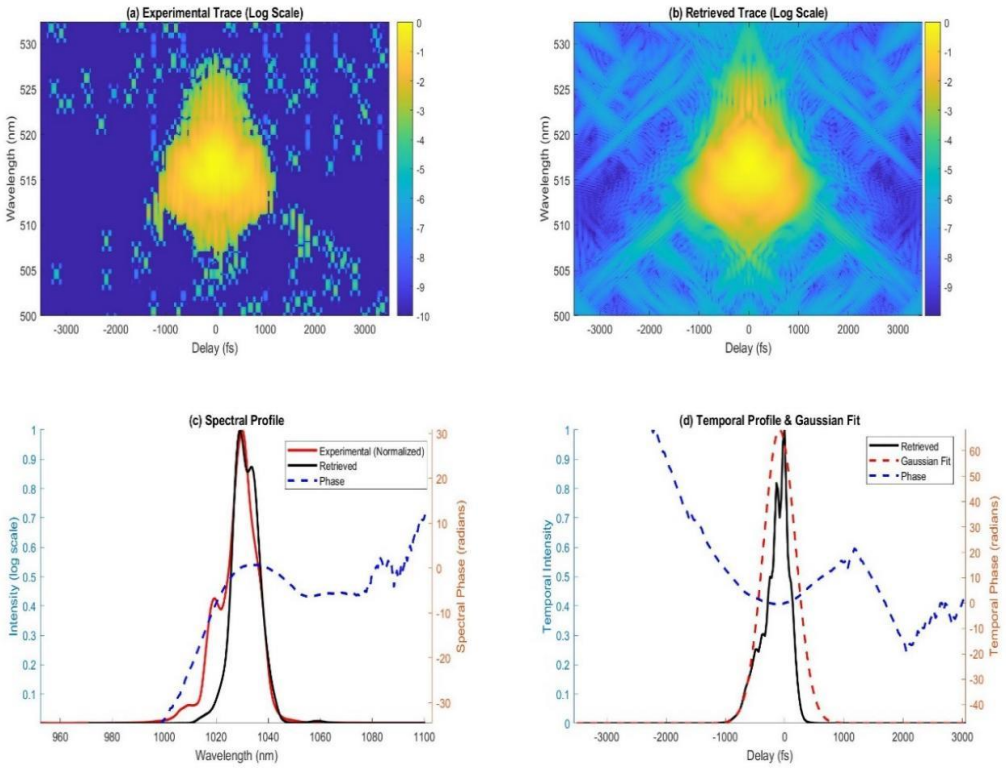

***Figure 5-2*- (a) Experimental FROG trace displaying measured intensity distribution as a function of delay and wavelength in log scale. The first Stokes shift corresponds to the center wavelength. Obtained from FROG retrieval systems, the retrieved trace (b) shows a successful reconstruction of the pulse properties and corresponds with the experimental trace. The retrieved spectrum in a solid black line is compared to the experimental spectrum in a solid red line and the spectral phase in a dashed blue line. Full width at half maximum (FWHM = 11.3 nm) shows the spectral bandwidth. The temporal intensity profile—solid black—is fitted with a Gaussian function (dashed red). With a well-compressed pulse shown by the observed pulse duration (FWHM = 396fs), effective energy transfer and minimum dispersion are suggested.**

Figure 5-2 represents original and retrieved FROG traces along with spectral and temporal profiles. The spectral profile of this pulse represents the first Stokes, which is centered around 1030 nm. Considering the initial pulse duration of 3000 fs, and the compressed pulse duration for the first Stokes (FWHM=396 fs), it can be implied that the pulse is compressed by a factor of$\sim$7.5. The intensity distribution and symmetry indicate minimal distortions in pulse shape. The color scale shows intensity, where the highest intensity regions are centered around zero delay, indicating a well-reconstructed pulse. The red dashed line shows a Gaussian fit, which is consistent with the obtained pulse, verifying a near-Gaussian profile.

Figure 5-3 represents the first Stokes pulse results at 3000 mbars, CH_4, initial pulse duration of 3 ps, and input energy of 2.5mJ.

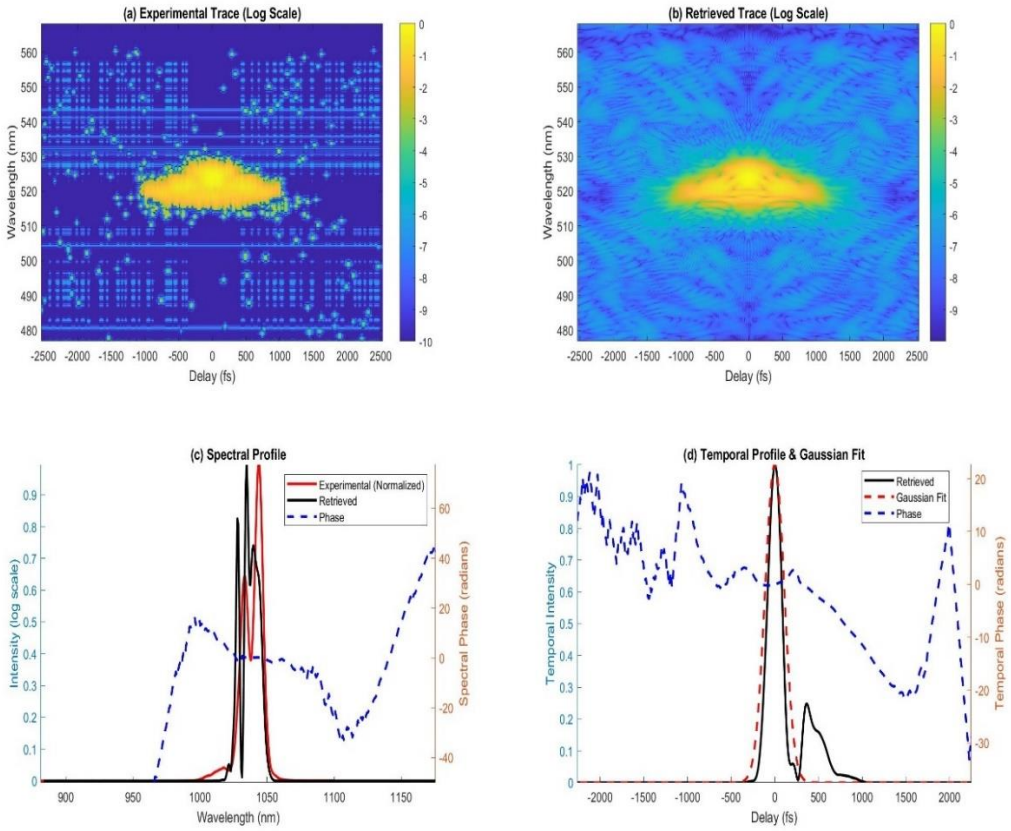

***Figure 5-3*- (a) Experimental trace and (b) Retrieved trace. (c) Spectral profile: The spectral bandwidth is FWHM = 19.6 nm. (d) Temporal profile: The retrieved temporal intensity (solid black) is compared with a Gaussian fit (dashed red). The pulse duration measured as FWHM=187 fs.**

Figure 5-3 represents the spectral and temporal profile along with the original and reconstructed traces of the compressed pulse. By comparing the pulse duration measured by FROG (FWHM=187 fs) to the input pulse duration (3000 fs), it can be concluded that the pulse has been compressed by a factor of ~17. Based on this result, it can be implied that without using dispersive elements, increasing pressure improves the compression process to some extent. In the following section, the role of dispersive elements has been explored.

Table 5-2 compares the FWHM pulse duration at 2000 mbar versus 3000 mbar of CH_4 at the same 2.5 mJ input energy and 3000 fs initial pulse. Spectral filters LP1000 and SP1326 (first Stokes) have been used.

***Table 5-2*: Output energy and RMS in the presence of different filters**

Pressure of CH_4 [mbar]	FWHM [fs]	Compression Factor
2000	559	~5.3
2000	376	~8
2000	284	~10.5
3000	201	~15
3000	196	~15.3
3000	181	~17

According to the result shown in Table 5-2, increasing pressure leads to a further shortening of pulse duration. Since increasing the pressure enhances the Raman gain, it leads to stronger and more coherent Stokes generation, which in turn broadens the spectrum of the Stokes pulse. A broader spectrum allows for a shorter pulse, increasing the compression factor.

5.3.2 Optimization of Pulse Compression Using Dispersive Mirrors and Bulk Materials

A FTL pulse can be achieved using chirped mirrors or gratings having specified GDD to compensate for the chirp of the pulse, resulting in a flat spectral phase. Due to the ambiguity of the SHG-FROG method in determining the sign of the chirp (i.e., whether the pulse is positively or negatively chirped), the next step involves evaluating pulse compression using a ZnSe glass window—a dispersive material that helps identify the chirp sign and optimizing the pulse compression process. The results below correspond to an experimental condition involving an initial pulse duration of 3 ps, 2000 mbar of CH_4, 2.5 mJ input energy, and the use of LP1000 and SP1325 to isolate the first Stokes. The results are presented in Table 5-3.

***Table 5-3:* Pulse duration (FHWH) for different thicknesses of ZnSe glass**

Optical Window	No Glass	1 mm ZnSe	5 mm ZnSe	11 mm ZnSe
Pulse Duration	180 fs	350 fs	450 fs	610 fs

The ZnSe glass shows a positive chirp at near infrared wavelengths (800nm-1100nm). From the refractive index info, at 1.01 μm GDD[2] for 1mm ZnSe is 663.95 fs^2. Since the pulse duration has been increased after adding 1mm ZnSe, it can be implied that the first Stokes pulse has residual positive chirp. (See figure 5-4).

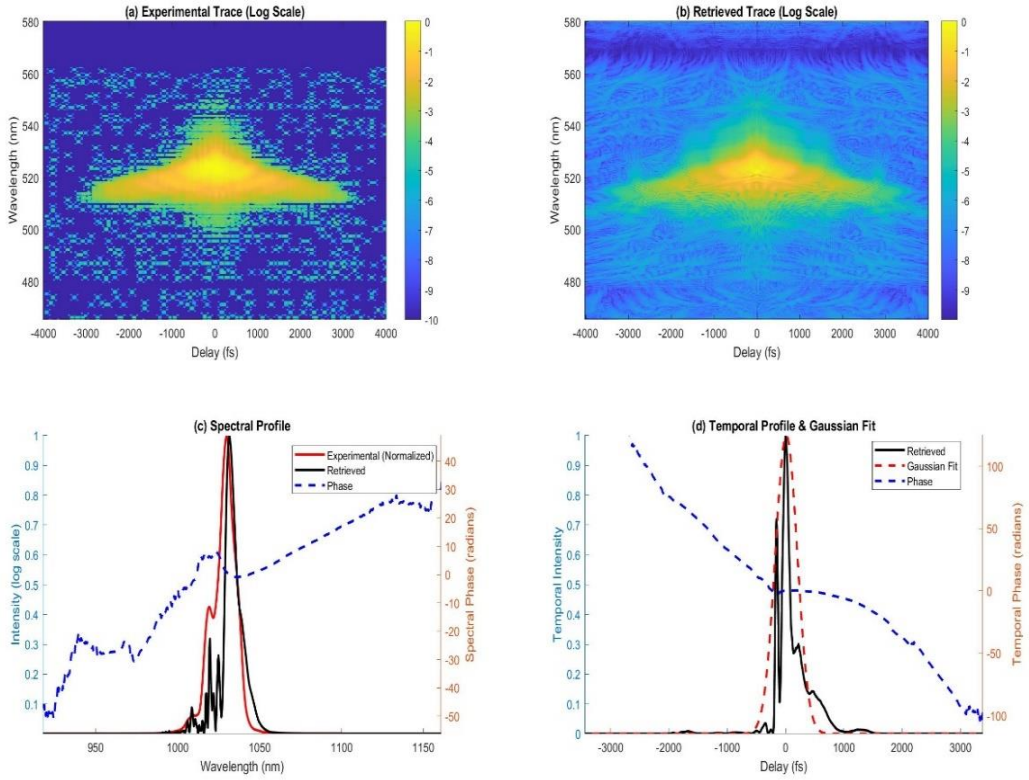

***Figure 5-4*- (a) Experimental trace and (b) Retrieved trace. (c) Spectral profile: The spectral bandwidth is FWHM = 7.6 nm. (d) Temporal profile: The pulse duration measured as FWHM is 350 fs.**

Original and reconstructed traces, as well as spectral and temporal profiles of the first Stokes pulse, are shown in Figure 5-4. The spectral profile of this pulse shows the first Stokes, which is centered around 1030 nm, as anticipated using relation (5.1). Due to the input pulse duration of 3000 fs, and the compressed pulse duration for the first Stokes (FWHM=350 fs), it can be concluded that the pulse is compressed by a factor of~ 9. Using the time-bandwidth product relation for a Gaussian pulse ($\Delta\nu_p \times \tau_p = 0.4413$) as discussed in section 3.5, and the spectral bandwidth of this first Stokes (7.6 nm), after calculating $\Delta\nu_p$, FTL is obtained as 204.8 fs. This calculation implies that obtaining the shortest pulse

[2] https://refractiveindex.info/

duration from an input pulse duration of 3000 fs to an FTL pulse duration of 204.8 (compression factor of$\sim$15) needs more depression compression.

5.4 Pulse Characterization of Second Stokes

We separated the second Stokes pulse by using two optical filters (LP1000 and SP1319). Figure 5-5 shows the results for the second Stokes under the experimental condition of 3000 mbar of CH_4, 2.5 mJ input energy and an initial pulse duration of 3000 fs. The successful operation of the Raman-based pulse-generating technique is confirmed by the second Stokes pulse showing spectrum broadening and temporal compression.

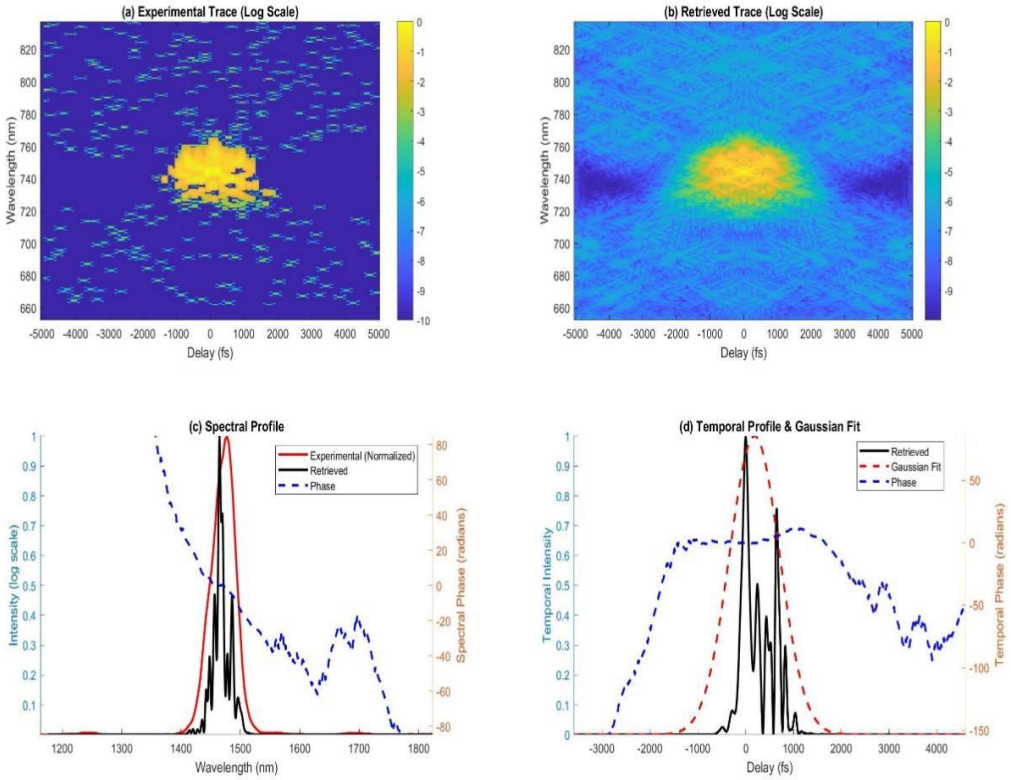

***Figure 5-5*- (a) Experimental trace and (b) Retrieved trace of the second Stokes pulse. (c) Spectral profile: FWHM=9.7 nm. (d) Temporal profile: The pulse duration measured as FWHM=790 fs.**

Figure 5-5 (a) shows experimental and reconstructed traces. The spectral profile of the second Stokes pulse is centered around 1470 nm (as anticipated in section 5.3) and the spectral bandwidth measured as FWHM=9.7 nm, suggesting modest spectral broadening that results from Raman interactions and SPM.

Although compression of the second Stokes result with a pulse duration of 790 fs (figure 5-5) is longer than the first Stokes pulse (previous results), it shows successful compression with a compression factor of around 4. The accuracy of phase reconstruction is confirmed by the well-matched retrieved pulse to the experimental measurement. Similar as calculating FTL for the first Stokes using the time-bandwidth product relation for a Gaussian pulse ($\Delta\nu_p \times \tau_p = 0.4413$), and the spectral bandwidth of this second Stokes pulse (9.7 nm), after calculating $\Delta\nu_p$, FTL can be calculated as 326.6 fs. The higher-order nonlinear interactions generating the second Stokes process are expected to result in broadening. While in this case the compression factor is ~4, the amount of FTL implies that from the input pulse duration of 3000 fs to the FTL pulse duration, dispersive elements that provide a compression factor of ~ 9 is required.

5.4.1 Energy Distribution and Conversion Efficiency of First and Second Stokes

To evaluate the efficiency of energy transfer from the pump to the Raman-shifted components, we measured the energy and stability of the first and second Stokes pulses. The results are summarized as follows at the experimental condition of input pulse duration of three ps, 2000 mbar of CH_4 and 2.5 mJ input energy.

Table 5-3: Energy and pulse duration of the first and second Stokes

Energy of the first Stokes and RMS	Energy of the second Stokes and RMS	Total Energy	FWHM Pulse Duration
E_{FS} =110.3 μJ RMS=9.7	E_{SS} =37.33 μJ RMS=35.33	1.376 mJ	First Stokes=350 fs Second stokes=790 fs

The total energy in the Stokes components is obtained by adding the individual contributions:

$$E_{stokes} = E_{FS} + E_{SS} = 110.3\mu J + 37.33\mu J = 147.63\mu J \quad (5.3)$$

Given the total input energy, the remaining unconverted pump energy is calculated as:

$$E_{Total} - E_{Stokes} = E_{Pump} \quad (5.4)$$

$$E_{Pump} = 1228.37\mu J$$

To determine the conversion efficiency of the first Stokes component relative to the pump, the following expression is used:

$$\frac{n_{FS}}{n_{Pump}} = \frac{E_1\lambda_1}{E_2\lambda_2} = \frac{110.3\times1030}{1228.37\times780} = \frac{113609}{958128.6} = 0.1185 \quad (5.5)$$

Where n_{FS} represents the number of first Stokes photons and n_{Pump} shows the number of pump photons. The efficiency percentage of the first Stokes is then obtained as:

$$\text{Conversion efficiency of the first Stokes} = \frac{n_{FS}}{n_{FS}+n_{Pump}} = \frac{113609}{1071737.6} = 0.106 \times 100 = 10.6\% \quad (5.6)$$

These results indicate that 10.6% of the total energy is efficiently transferred to the first Stokes component, while the remaining energy is either retained in the pump or transferred to higher-order Stokes waves. Furthermore, the higher RMS of the second Stokes (35.33%) indicates greater instability in energy fluctuations compared to the first Stokes (9.7%). These findings show effective performance of Raman frequency conversion, the stability of generated Stokes components, and the overall energy dynamics within the experimental setup. Using a similar calculation, the conversion efficiency for the second Stokes with a central wavelength of λ=1470 nm is calculated as 5.41 %, indicating that 5.41% of the total energy is efficiently transferred to the second Stokes component.

These results indicate that different filter combinations significantly affect the output energy and stability (RMS). The highest stability was observed for the combination of LP1000 and SP1325 (RMS = 10.18%), while the combination of LP1000 and LP1319 showed the highest instability (RMS = 35.33%). The total unfiltered output energy was 1.387 mJ, with an RMS of 13.23%, providing a reference for energy losses introduced by the filtering process.

5.5 Challenges in Generation First and Second Stokes

Based on this thesis's experimental results, several challenges can be identified in generating and compressing the first and second Stokes pulses using vibrational SRS in CH_4. On one hand, RMS energy fluctuation for the first Stokes remained below a 10% range, which is moderate but still limits precision applications. The first Stokes generation saturates at high pressure and input energy combinations; increasing energy no longer increases output proportionally, which indicates limits to energy scaling without mode instability or nonlinear effects like SPM becoming dominant. On the other hand, the second Stokes was generated at a lower energy efficiency than the first Stokes. RMS fluctuations for the second Stokes were >25%, reaching up to 30% in some experiments, which indicates temporal and spatial instability due to phase mismatching and modal dispersions. Another challenge in dealing with the second Stokes is that after compression, the second Stokes pulse duration remained longer (FWHM=790 fs),

indicating incomplete compression or more residual dispersion. Finally, small deviations in alignment caused large swings in output energy and pulse duration for both first and second Stokes.

6 CONCLUSION AND FUTURE OUTLOOK

This thesis investigates the generation and compression of ultrashort laser pulses using a 780 nm Ti: Sapphire pump laser propagating in a CH_4-filled HCF based on the SRS effect. The newly generated wavelengths, known as first and second Stokes, have been characterized using FROG.

This study's motivation was to access longer-wavelength laser sources. Conventional solid-core optical fibers made from silica-based materials are limited in energy scalability due to their low damage threshold, resulting in limited frequency shifts. Therefore, one alternative way to overcome this limitation is to use vibrational Stimulated Raman Scattering using CH_4 as a nonlinear medium, which enables access to larger vibrational frequency shifts. Hydrogen provides the largest shift; however, the disadvantage is that the rotational effect can interfere with the vibrational SRS. On the other hand, CH_4 is a symmetric top molecule and does not generate the rotational Raman signal, making it a promising nonlinear medium for vibrational SRS. First and second Stokes pulses were generated by precisely optimizing the experimental parameters, including gas pressure, grating position, input energy, and beam alignment.

Because of the ambiguity of the SHG-FROG method in determining the chirp pulse after propagating through the fiber, a ZnSe glass with a determined amount of GDD at a specific wavelength is used to identify the chirp sign. Our results indicate that the maximum compression factor that we achieved for the first Stokes was ~ 17, while the compression factor for the second Stokes was ~ 4. Effective energy redistribution in the Raman process is demonstrated by first and second Stokes pulse conversion efficiencies of 10.6% and 5.41%, respectively.

These results pave the way for optimizing ultrashort Raman-based wavelength conversion systems, which have applications in high-speed optical communication, nonlinear optics, and mid-IR generation. By optimizing gas pressure, fiber length, and alignment conditions, such as utilizing longer HCFs or pressure-graded HCFs to extend nonlinear interaction length, efficiency and stability can be further improved without introducing excessive loss. Moreover, exploring a mixture of CH_4 and H_2 would be beneficial to access large vibrational shifts as well as strong Raman gain, while mitigating the rotational effect. Further exploration using alternative pump lasers, such as a Yb-based laser at 1030 nm, may also broaden the spectrum into the mid-infrared region.

REFERENCES

1. DiDomenico Jr, M., et al., *Generation of ultrashort optical pulses by mode locking the YAIG: Nd laser.* Applied Physics Letters, 1966. **8**(7): p. 180-183.
2. Haus, H.A., *Mode-locking of lasers.* IEEE Journal of Selected Topics in Quantum Electronics, 2000. **6**(6): p. 1173-1185.
3. Krausz, F., *Attosecond science comes of age*, in *Attosecond Physics (Springer Series in Optical Sciences).* 2013, Springer. p. 257-270.
4. Wise, F.W., A. Chong, and W.H. Renninger, *High-energy femtosecond fiber lasers based on pulse propagation at normal dispersion.* Laser & Photonics Reviews, 2008. **2**(1-2): p. 58-73.
5. Brabec, T., et al., *Kerr lens mode locking.* Optics letters, 1992. **17**(18): p. 1292-1294.
6. Strickland, D. and G. Mourou, *Compression of amplified chirped optical pulses.* Optics communications, 1985. **55**(6): p. 447-449.
7. Martinez, O., *3000 times grating compressor with positive group velocity dispersion: Application to fiber compensation in 1.3-1.6 μm region.* IEEE Journal of Quantum Electronics, 1987. **23**(1): p. 59-64.
8. Jeong, J., et al., *Modeling and Analysis of High-Power Ti: sapphire Laser Amplifiers–A Review.* Applied Sciences, 2019. **9**(12): p. 2396.
9. Shimizu, F., *Frequency broadening in liquids by a short light pulse.* Physical Review Letters, 1967. **19**(19): p. 1097.
10. Li, C., *Nonlinear optics.* Principles and Applications, 2017.
11. Alfano, R.R. and S. Shapiro, *Observation of self-phase modulation and small-scale filaments in crystals and glasses.* Physical Review Letters, 1970. **24**(11): p. 592.
12. Zheltikov, A.M., *Ultrashort light pulses in hollow waveguides.* Physics-Uspekhi, 2002. **45**(7): p. 687.
13. Mohammadabadi, R.S., *Towards the Advanced High-Energy Multidimensional Laser Technology Through Harnessing the Spatiotemporal Nonlinear Enhancement*. 2020, Institut National de la Recherche Scientifique (Canada).
14. DeLong, K., et al., *Frequency-resolved optical gating with the use of second-harmonic generation.* Journal of the Optical Society of America B, 1994. **11**(11): p. 2206-2215.
15. Miles, R., G. Laufer, and G. Bjorklund, *Coherent anti-Stokes Raman scattering in a hollow dielectric waveguide.* Applied Physics Letters, 1977. **30**(8): p. 417-419.
16. Trebino, R., et al., *Measuring ultrashort laser pulses in the time-frequency domain using frequency-resolved optical gating.* Review of Scientific Instruments, 1997. **68**(9): p. 3277-3295.
17. Cho, Y.C. and S.I. Ahn, *Fabricating a Raman spectrometer using an optical pickup unit and pulsed power.* Scientific reports, 2020. **10**(1): p. 11692.
18. Benabid, F., et al., *Stimulated Raman scattering in hydrogen-filled hollow-core photonic crystal fiber.* Science, 2002. **298**(5592): p. 399-402.
19. Diels, J.-C., E. Van Stryland, and G. Benedict, *Generation and measurement of 200 femtosecond optical pulses.* Optics Communications, 1978. **25**(1): p. 93-96.
20. Fork, R.L., et al., *Compression of optical pulses to six femtoseconds by using cubic phase compensation.* Optics letters, 1987. **12**(7): p. 483-485.
21. Moulton, P.F., *Spectroscopic and laser characteristics of Ti: Al2O3.* Journal of the Optical Society of America B, 1986. **3**(1): p. 125-133.
22. Nisoli, M., et al., *Compression of high-energy laser pulses below 5 fs.* Optics letters, 1997. **22**(8): p. 522-524.

23. Chauhan, V., et al., *Single-diffraction-grating and grism pulse compressors.* Journal of the Optical Society of America B, 2010. **27**(4): p. 619-624.
24. Samad, R., et al., *Ultrashort laser pulses applications*, in *Coherence and Ultrashort Pulse Laser Emission*. 2010, IntechOpen.
25. Hecht, J., *Short history of laser development.* Optical engineering, 2010. **49**(9): p. 091002-091002-23.
26. Keller, U. and R. Paschotta, *Ultrafast lasers*. 2021: Springer.
27. Courtney, T.L., et al., *Optimization of stimulated rotational Raman scattering over vibrational scattering in a hydrogen-filled fiber.* Opt Lett, 2024. **49**(14): p. 3926-3929.
28. Pickering, J.D., *Ultrafast lasers and optics for experimentalists*. 2024: IOP Publishing.
29. French, P., *The generation of ultrashort laser pulses.* Reports on Progress in Physics, 1995. **58**(2): p. 169.
30. Chvykov, V., *High-Power Lasers.* Encyclopedia, 2024. **4**(3): p. 1236-1249.
31. Yusoff, Z., et al., *A 36-channel x 10-GHz spectrally sliced pulse source based on supercontinuum generation in normally dispersive highly nonlinear holey fiber.* IEEE Photonics Technology Letters, 2003. **15**(12): p. 1689-1691.
32. Khalifeh Soltanian, S.M.J., *High pulse to pulse stability high power femtosecond Yb-doped fiber laser*. 2023, Université du Québec, Institut national de la recherche scientifique.
33. Zewail, A.H., *Femtochemistry: Atomic-scale dynamics of the chemical bond.* The Journal of Physical Chemistry A, 2000. **104**(24): p. 5660-5694.
34. Boyd, R.W., A.L. Gaeta, and E. Giese, *Nonlinear optics*, in *Springer Handbook of Atomic, Molecular, and Optical Physics*. 2008, Springer. p. 1097-1110.
35. Agrawal, G.P., *Fiber-optic communication systems*. 2012: John Wiley & Sons.
36. Galli, I., et al., *Mid-infrared frequency comb for broadband high precision and sensitivity molecular spectroscopy.* Optics letters, 2014. **39**(17): p. 5050-5053.
37. Inoue, T. and S. Namiki, *Pulse compression techniques using highly nonlinear fibers.* Laser & Photonics Reviews, 2008. **2**(1-2): p. 83-99.
38. Stolen, R.H. and C. Lin, *Self-phase-modulation in silica optical fibers.* Physical Review A, 1978. **17**(4): p. 1448.
39. Finot, C. and J. Fatome, *All-optical fiber-based ultrafast amplitude jitter magnifier.* Optics Express, 2010. **18**(18): p. 18697-18702.
40. Finot, C. and J. Fatome, *Experimental demonstration of an ultrafast all-optical bit-error indicating scheme.* Microwave and Optical Technology Letters, 2011. **53**(2): p. 392-395.
41. Markaryan, N., L.K. Muradyan, and T. Papazyan, *Spectral compression of ultrashort laser pulses.* Soviet journal of quantum electronics, 1991. **21**(7): p. 783.
42. Richardson, D.J., J. Nilsson, and W.A. Clarkson, *High power fiber lasers: current status and future perspectives.* Journal of the optical society of America B, 2010. **27**(11): p. B63-B92.
43. Gustafson, T., P. Kelly, and R. Fisher, *Subpicosecond pulse generation using the optical Kerr effect.* IEEE Journal of Quantum Electronics, 1969. **5**(6): p. 325-325.
44. Agrawal, G.P., *Nonlinear fiber optics*, in *Nonlinear Science at the Dawn of the 21st Century*. 2000, Springer. p. 195-211.
45. Dudley, J., A. Peacock, and G. Millot, *The cancellation of nonlinear and dispersive phase components on the fundamental optical fiber soliton: a pedagogical note.* Optics communications, 2001. **193**(1-6): p. 253-259.
46. Chung, H.-Y., et al., *Megawatt peak power tunable femtosecond source based on self-phase modulation enabled spectral selection.* Optics express, 2018. **26**(3): p. 3684-3695.
47. Buldt, J., et al., *Temporal contrast enhancement of energetic laser pulses by filtered self-phase-modulation-broadened spectra.* Optics Letters, 2017. **42**(19): p. 3761-3764.

48. Lin, C. and T. Gustafson, *Optical pulsewidth measurement using self-phase modulation.* IEEE Journal of Quantum Electronics, 1972. **8**(4): p. 429-430.
49. Baudin, K., F. Audo, and C. Finot, *Fiber-based measurement of temporal intensity and phase profiles of an optical telecommunication pulse through self-phase modulation.* Microwave and Optical Technology Letters, 2018. **60**(4): p. 882-886.
50. Kim, K., et al., *Measurement of the nonlinear index of silica-core and dispersion-shifted fibers.* Optics letters, 1994. **19**(4): p. 257-259.
51. Liu, M. and P. Wang, *Principles and Applications of.* Optical Communications, IRWM, 1996. **415**.
52. Tomlinson, W., R. Stolen, and C. Shank, *Compression of optical pulses chirped by self-phase modulation in fibers.* Journal of the Optical Society of America B, 1984. **1**(2): p. 139-149.
53. Vozzi, C., et al., *Optimal spectral broadening in hollow-fiber compressor systems.* Applied Physics B, 2005. **80**(3): p. 285-289.
54. Witte, S. and K.S. Eikema, *Ultrafast optical parametric chirped-pulse amplification.* IEEE Journal of Selected Topics in Quantum Electronics, 2011. **18**(1): p. 296-307.
55. Nisoli, M., S. De Silvestri, and O. Svelto, *Generation of high energy 10 fs pulses by a new pulse compression technique.* Applied Physics Letters, 1996. **68**(20): p. 2793-2795.
56. Cardin, V., et al., *0.42 TW 2-cycle pulses at 1.8 μm via hollow-core fiber compression.* Applied Physics Letters, 2015. **107**(18).
57. Ell, R., et al., *Generation of 5-fs pulses and octave-spanning spectra directly from a Ti: sapphire laser.* Optics letters, 2001. **26**(6): p. 373-375.
58. Niu, H., et al., *Dispersive mirrors for high third-order dispersion compensation in femtosecond amplification fiber laser system.* Applied Physics B, 2012. **108**: p. 609-614.
59. Chi, H., et al., *Nonlinearity optimization of dissipative-soliton fiber laser for generation of pulses with 350 kW peak power.* High Power Laser Science and Engineering, 2018. **6**: p. e27.
60. Xie, C., et al., *Vector-dispersion compensation and pulse pedestal cancellation in a femtosecond nonlinear amplification fiber laser system.* Optics letters, 2011. **36**(21): p. 4149-4151.
61. Fernández, A., et al., *High-fidelity, 160 fs, 5 μJ pulses from an integrated Yb-fiber laser system with a fiber stretcher matching a simple grating compressor.* pulse, 2012. **5**: p. 12.
62. Brabec, T. and F. Krausz, *Intense few-cycle laser fields: Frontiers of nonlinear optics.* Reviews of Modern Physics, 2000. **72**(2): p. 545.
63. Nisoli, M., et al., *A novel-high energy pulse compression system: generation of multigigawatt sub-5-fs pulses.* Applied Physics B: Lasers & Optics, 1997. **65**(2).
64. Kane, D.J. and R. Trebino, *Characterization of arbitrary femtosecond pulses using frequency-resolved optical gating.* IEEE Journal of Quantum Electronics, 1993. **29**(2): p. 571-579.
65. Trebino, R., et al., *Highly reliable measurement of ultrashort laser pulses.* Journal of Applied Physics, 2020. **128**(17).
66. Paschotta, R., *Frequency-resolved Optical Gating*.
67. Trebino, R., *Frequency-Resolved Optical Gating: The Measurement of Ultrashort Laser Pulses: The Measurement of Ultrashort Laser Pulses*. 2000: Springer Science & Business Media.
68. Chen, Y.-H., et al., *Efficient soliton self-frequency shift in hydrogen-filled hollow-core fiber.* Optics Letters, 2022. **47**(2): p. 285-288.